Performance Analysis of NOMA Under Practical Constraints and Noise Variability

M.Tech Thesis

by

DIVYANSHI SINGH

DEPARTMENT OF ELECTRICAL ENGINEERING
INDIAN INSTITUTE OF TECHNOLOGY INDORE
MAY 2025

Performance Analysis of NOMA Under Practical Constraints and Noise Variability

A THESIS

Submitted in partial fulfillment of the

requirements for the award of the degree

of

MASTER OF TECHNOLOGY

by

DIVYANSHI SINGH

DEPARTMENT OF ELECTRICAL ENGINEERING
INDIAN INSTITUTE OF TECHNOLOGY INDORE
MAY 2025

INDIAN INSTITUTE OF TECHNOLOGY INDORE

CANDIDATE'S DECLARATION

I hereby certify that the work which is being presented in the thesis entitled "**Performance Analysis of NOMA Under Practical Constraints and Noise Variability**" in the partial fulfillment of the requirements for the award of the degree of **MASTER OF TECHNOLOGY** and submitted in the **DEPARTMENT OF ELECTRICAL ENGINEERING**, **Indian Institute of Technology Indore**, is an authentic record of my own work carried out during the time period from July 2023 to May 2025 under the supervision of Prof. Vimal Bhatia, Professor, Department of Electrical Engineering, Indian Institute of Technology Indore, India.

The matter presented in this thesis has not been submitted by me for the award of any other degree of this or any other institute.

Divyanshi 22/05/2025

Signature of the student with date

(DIVYANSHI SINGH)

This is to certify that the above statement made by the candidate is correct to the best of my/our knowledge.

22.05.2025

Signature of Thesis Supervisor with date

(Prof. VIMAL BHATIA)

DIVYANSHI SINGH has successfully given her M.Tech. Oral Examination held on ...

Saptarshi Ghosh

Convener, DPGC

Date: 22-05-2025

22.05.2025

Signature of Thesis Supervisor with date

(Prof. VIMAL BHATIA)

ACKNOWLEDGEMENTS

I take this opportunity to acknowledge my heartfelt gratitude to all those who have directly or indirectly helped me throughout my MTech. First and foremost, I thank God Almighty for giving me the strength, knowledge, and enlightenment to undertake this research work. Then, I would like to express my deep sense of respect and gratitude to my supervisor and mentor, Prof. Vimal Bhatia, for his invaluable guidance, sustained inspiration, and kind support towards my thesis work. He has given me all the freedom to pursue my research, and provided helpful career advice and suggestions, extending beyond academic boundaries, whenever needed.

Next, I am thankful to all the faculty members and the staff at IIT Indore for their cooperation throughout my thesis work.

Many thanks to Mr. Amit Baghel for his cooperation in the project and helping in writing this thesis. This really couldn't have been possible without his immense help and support. My appreciation also goes to all the members of the Signal and Software Group for creating a friendly and conductive environment.

I am extremely thankful to all my batchmates and hostel unitmates for making a wonderful company and sharing all the casual and valued moments which helped me during the hardship of this work and my life at IIT Indore.

I would like to thank the Ministry of Human Resource Development (MHRD), Government of India and IIT Indore for providing financial assistance. I will also thank the finance, administration, academic, and R&D sections for all the necessary support.

Lastly, above all, the most valued gratitude is expressed for my family for their endless support and faith in me, without which I would have not been able to achieve the greatest milestone of my life.

DIVYANSHI SINGH

ABSTRACT

The rapid growth of wireless connectivity, expected to intensify with the advent of next-generation wireless technologies, brings a substantial increase in the number of connected users. Given the physical limitations of bandwidth expansion, there is a critical need for communication strategies that efficiently accommodate this expanding user base within finite spectral resources.

Traditionally, Orthogonal Multiple Access (OMA) techniques have addressed bandwidth limitations by assigning distinct resources to each user. However, as user density increases, the rigid orthogonality of OMA becomes a constraint, particularly for emerging wireless systems. In contrast, Non-Orthogonal Multiple Access (NOMA) offers a more flexible solution by enabling multiple users to share the same time-frequency resources. Through the use of superposition coding and power domain separation, NOMA improves spectral efficiency and supports massive connectivity. User signals are differentiated via power levels and decoded using successive interference cancellation (SIC), making it a promising candidate for 5G and beyond.

As wireless communication evolves toward sixth-generation (6G) networks, the demand for enhanced spectral efficiency, energy efficiency, and massive connectivity intensifies. NOMA stands out as a strong contender to meet these requirements. However, several practical challenges hinder its real-world implementation, including multi-user interference, error propagation in SIC, imperfect channel state information (CSI), and transceiver hardware impairments (HIs).

This thesis investigates the integration of NOMA under realistic system constraints, focusing on the impact of imperfect CSI and hardware impairments. Furthermore, the performance of NOMA is analyzed in two distinct noise environments: Additive White Gaussian Noise (AWGN) and impulsive noise. By addressing these challenges and conditions, the study aims to evaluate the practical viability and performance trade-offs of NOMA in future wireless networks.

Contents

List of Figures

List of Symbols

- Basic arithmetic and calculus notations have standard definitions.

Elementary & Special Functions

Notation	Definition
$\Gamma(\cdot)$	Gamma function
$\Upsilon(\cdot,\cdot)$	lower incomplete Gamma function
$I_v(.)$	modified v-order Bessel function of the first kind
$\log_i(\cdot)$	logarithm to base i

Probability & Statistics

Let X be a random variable, and $\mathcal{A}$ be an arbitrary event.

Notation	Definition
$E\{\cdot\}$	expectation
$f_X(\cdot)$	probability density function (PDF) of X
$F_X(\cdot)$	cumulative distribution function (CDF) of X
$\Pr\{\mathcal{A}\}$	probability of $\mathcal{A}$
$X \sim \mathcal{CN}(\mu, \sigma^2)$	X is complex Gaussian distributed with mean μ and variance σ^2

Miscellaneous

Notation	Definition
$\lvert\cdot\rvert$	absolute value
$[x]^+$	$\max\{x, 0\}$
$n!$	factorial of n

Acronyms

5G	Fifth-Generation
6G	Sixth-Generation
AWGN	Additive White Gaussian Noise
BS	Base Station
CDF	Cumulative Distribution Function
PBS	Pico Base Stations
MBS	Macro Base Station
CSI	Channel State Information
IpCSI	Imperfect Channel State Information
HI	Hardware Impairements
EE	Energy Efficiency
Im-N	Impulsive Noise
BER	Bit Error Rate
LoS	Line-of-Sight
NOMA	Non-Orthogonal Multiple Access
OMA	Orthogonal Multiple Access
PDF	Probability Density Function
OP	Outage Probability
RF	Radio-Frequency
RIS	Reconfigurable Intelligent Surfaces
SC	Superposition Coding
SIC	Successive Interference Cancellation
SINR	Signal-to-Interference-Plus-Noise Ratio
SWIPT	simultaneous wireless information and power transfer.
SNR	Signal-to-Noise Ratio

CHAPTER 1

INTRODUCTION AND BACKGROUND

1.1 Evolution of Wireless Communications: From 1G to 6G.

The evolution of wireless communication systems represents one of the most significant technological advancements in modern history, underpinning the development of mobile connectivity, data transmission, and digital transformation across various sectors. Since the inception of the first-generation (1G) analog cellular networks in the late 20th century, each subsequent generation has introduced substantial improvements in terms of spectral efficiency, latency, data rates, mobility, reliability, and network capacity.

1G networks, based on analog frequency modulation, operated in the 800–900 MHz bands and were primarily designed for voice communication, with limited channel capacity, poor voice quality, and no encryption. The transition to 2G, built on digital technologies such as GSM, CDMA, and TDMA, introduced circuit-switched data, enhanced voice quality, SMS services, and significantly improved spectrum utilization.

With the arrival of 3G (e.g., UMTS, CDMA2000), the focus shifted to higher data throughput and multimedia support, leveraging technologies like WCDMA and HSPA. These networks introduced packet-switched data and enabled early mobile internet access with peak downlink speeds of up to several Mbps. 4G LTE networks marked a paradigm shift with an all-IP architecture, employing OFDMA and MIMO technologies to achieve significantly higher data rates, lower latency, and improved quality of service (QoS) for real-time applications such as HD video streaming and

VoIP.

5G, standardized under 3GPP Release 15 and beyond, brings transformative capabilities including enhanced mobile broadband (eMBB), ultra-reliable low-latency communication (URLLC), and massive machine-type communication (mMTC). It utilizes sub-6 GHz and mmWave frequencies, beamforming, network slicing, and edge computing to meet the demands of Industry 4.0, autonomous systems, and IoT ecosystems.

Looking forward, 6G is envisioned as a fully intelligent and integrated communication fabric that extends beyond mobile connectivity. Anticipated to operate in the sub-THz and THz spectrum, 6G aims to offer data rates exceeding 1 Tbps, sub-millisecond latency, extreme energy efficiency, and support for real-time holographic communications, AI-native networking, and brain-computer interfaces. Emerging enablers include reconfigurable intelligent surfaces (RIS), quantum communication elements, and integrated sensing and communication (ISAC) capabilities.

This thesis provides an in-depth technical analysis of the progression from 1G to 6G, discussing the enabling technologies, performance metrics, frequency utilization, standardization efforts, and the architectural evolution that has shaped the wireless landscape. Special emphasis is placed on the trade-offs, challenges, and research frontiers associated with each generational shift.

1.2 Non-orthoganal Multiple Access Technique

The core idea behind NOMA is the utilization of the power domain to enable multiple user access, as shown in Figure 1.1. In contrast to traditional multiple access methods, NOMA incorporates power-level differentiation to allow signal multiplexing within the existing domains of time, frequency, or code. Essentially, NOMA functions as a complementary enhancement to current multiple access techniques, with the capability to boost both spectral efficiency and user connectivity. The core technologies that enable NOMA are SC and SIC. These techniques have advanced greatly, making NOMA practical for next-generation networks. In NOMA, the base station transmits a composite signal by superimposing the coded messages of multiple users using SC. A more detailed survey of uplink and downlink NOMA schemes and their integration into 5G frameworks is discussed in [1].

User selection is also vital and typically depends on channel gains and quality-

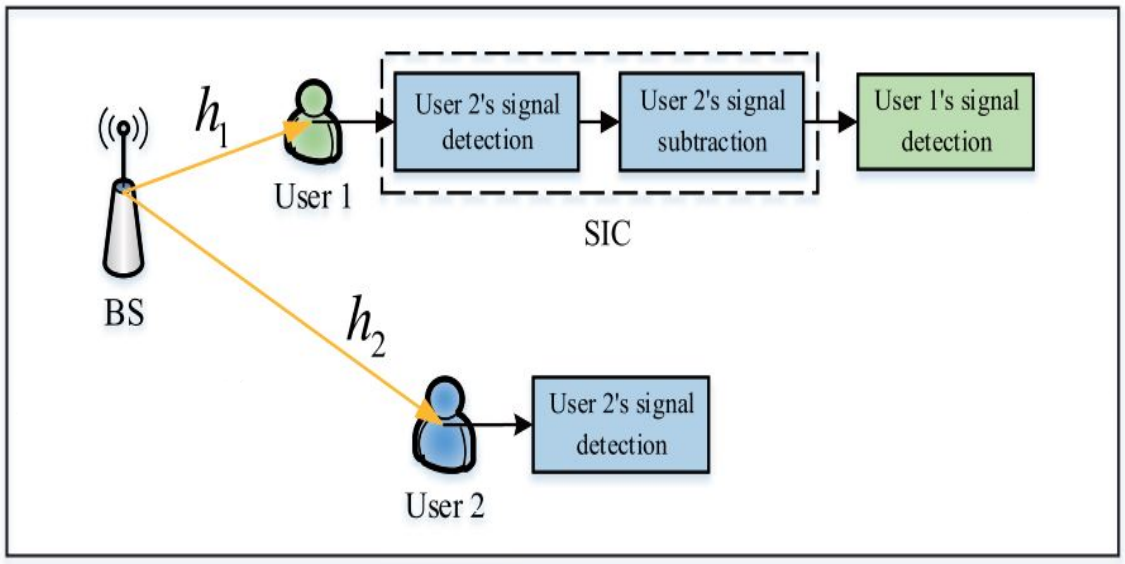

Figure 1.1: Illustration of downlink power domain NOMA transmission [2]

of-service (QoS) requirements. Users are often paired based on differing channel conditions—for example, a near user with a strong signal is paired with a far user with a weaker one. The far user is allocated more power to decode its message while treating others as interference. Meanwhile, the near user uses SIC to remove the far user's signal before decoding its own.

When users have similar channel conditions, QoS demands guide pairing and power allocation—users with stricter latency, reliability, or throughput needs may be prioritized. Unlike traditional orthogonal multiple access (OMA) that uses schemes like water-filling, NOMA reverses this by giving more power to users with weaker channels, ensuring reliable decoding and improved system performance.

1.2.1 SIC

SIC is a decoding technique used in NOMA to separate overlapping signals from multiple users. In this process, the receiver first decodes the signal with higher power typically assigned to the user with a weaker channel. After successfully decoding it, the receiver subtracts that signal from the combined transmission, making it easier to decode the remaining lower-power signals. This step-by-step removal of interference enables efficient decoding of multiple user messages sharing the same time and frequency resources.

1.2.2 SC

SC is a technique used in communication systems, particularly in the context of multi-user environments, to improve efficiency. It involves encoding multiple messages simultaneously over the same frequency spectrum, by layering or "superimposing" these signals on top of each other. Each user's message is transmitted in such a way that it occupies the same time and frequency resources, but each signal is structured differently. The receiver, aware of the structure of the different signals, can decode and separate the superimposed messages. This allows for more efficient use of available resources, enabling the transmission of more data in the same bandwidth. In essence, superposition coding leverages the ability to overlap signals in a way that maximizes the use of the channel while minimizing interference.

1.3 Wireless Channel: Modeling and Performance Metrices

The wireless communication channel serves as the pathway for transmitting information signals from the source to the destination. These signals experience various impairments as they propagate. This section covers the basics of wireless propagation, multipath fading, and different channel models. Additionally, it provides an explanation of key performance metrics for wireless systems, along with their mathematical formulations, to help evaluate system performance.

1.3.1 Modeling of Wireless Channel

Fading in wireless communication refers to the variations in signal strength that occur as a result of the signal's propagation through the environment. These variations are typically caused by obstacles, interference, and reflections that the signal encounters as it travels from the transmitter to the receiver. Fading plays a critical role in modeling the wireless channel because it affects the quality of the received signal and, consequently, the performance of the communication system.

When modeling a wireless channel, fading is usually represented as a random process, meaning that the received signal strength can fluctuate unpredictably. The primary types of fading models used to describe these variations include:

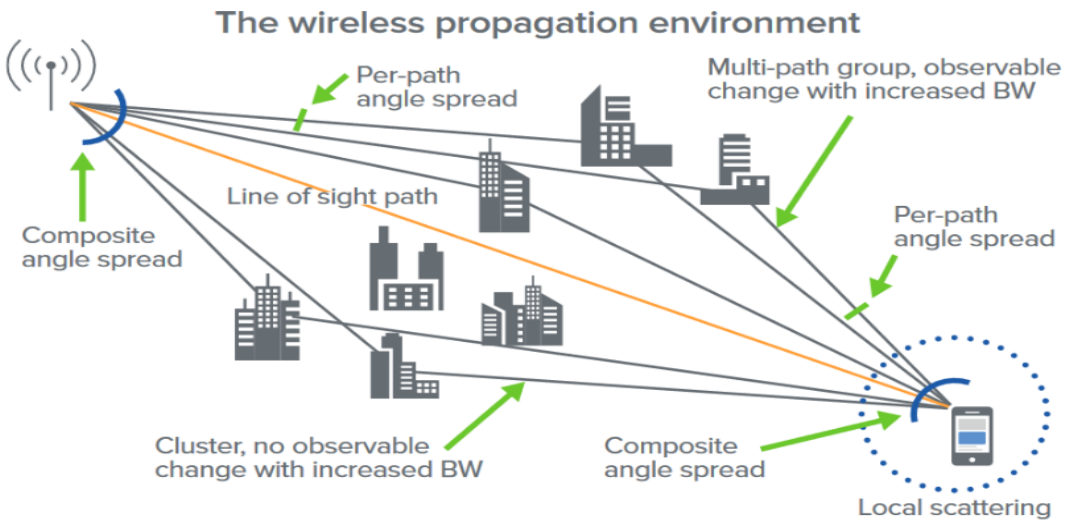

Figure 1.2: Wireless Communication fading channels.[3]

Small-scale fading results from rapid changes in the signal due to multipath propagation, where reflected signals combine constructively or destructively. Large-scale fading, on the other hand, occurs over longer distances due to factors like path loss from obstacles and terrain. Multipath fading, a subset of small-scale fading, is caused by signals arriving at slightly different times, leading to interference patterns. The Doppler shift, caused by movement of the transmitter, receiver, or surrounding objects, further impacts the signal by altering its frequency. To model these effects, statistical approaches like Rayleigh fading (used when there's no line-of-sight) and Ricean fading (used when a strong line-of-sight path is present) are commonly applied.

Rayleigh Fading is widely used to characterize the statistical behavior of radio channels, particularly in scenarios where multipath propagation occurs without a dominant line-of-sight (LoS) path between the base station and end users. In such environments, the received signal results from the constructive and destructive interference of multiple reflected paths. As a result, its in-phase and quadrature components are modeled as zero-mean complex Gaussian random processes. Consequently, the amplitude of the received signal follows a Rayleigh distribution.

Ricean Fading is typically used when a prominent stationary non-line-of-sight (non-LoS) component exists between the end users. In such scenarios, the multipath signal gains a direct current (DC) component due to the superposition of the

reflected paths, leading to a dominant, stationary, non-fading signal component. When this strong LoS component is absent, the Rician distribution simplifies to the Rayleigh distribution as a special case.

Nakagami-m is commonly employed to model small-scale fading in environments with dense signal scattering. Its flexibility makes it suitable for various real-world applications, including wireless communication and radio wave propagation. Thanks to its generalized fading characteristics, it can represent different fading conditions based on the value of the shape parameter m. Notably, for $m = \frac{1}{2}$, it reduces to a one-sided Gaussian distribution, and for $m = 1$, it becomes equivalent to the Rayleigh distribution.

1.3.2 Performance Metrices

To evaluate the performance of wireless communication systems over fading channels, various performance metrics are employed across different modulation schemes. These metrics help address key design challenges in wireless system development. Commonly used measures include instantaneous SNR, outage probability, system throughput, energy efficiency, ergodic capacity, and average symbol error rate.

Instantaneous SNR is a fundamental metric used to assess the degradation of a signal caused by noise. It plays a critical role in data detection, as it is measured at the receiver's output and serves as a reliable indicator of the overall fidelity of the communication system. Mathematically, the instantaneous SNR is defined as:

$$\gamma = \frac{\text{Received signal power}}{\text{Received noise power}} = \frac{P|h|^2}{\sigma^2} \tag{1.1}$$

where P denotes the transmit power, h is the channel coefficient, and σ^2 represents the noise variance.

In wireless communication systems, due to the presence of multipath fading, the **average SNR** is often a more representative performance metric than the instantaneous SNR. The average SNR accounts for the statistical variations in the fading channel and is defined as:

$$\Omega = \mathbb{E}[\gamma]$$

where $\mathbb{E}[\cdot]$ denotes the statistical expectation operator.

Outage Probability is a key performance metric that represents the likelihood of a link failure, particularly in slow-fading scenarios. It is defined as the probability that the received end-to-end instantaneous SNR, denoted by γ, falls below a predefined threshold γ_{th}.

System Throughput System throughput is a crucial performance metric used to characterize spectrum utilization, and it is often referred to as the mean spectral efficiency. Based on the derived expression for outage probability (P_{out}), the system throughput can be expressed as:

$$\tau = [1 - P_{\text{out}}(\gamma_{\text{th}})]\, r_{\text{th}}$$

Energy Efficiency is a key performance metric in wireless communication systems, playing a crucial role in realizing the vision of green communication. It is defined as the ratio of the total data transferred to the total energy consumed. The total data transferred is represented by the system throughput. Energy efficiency can be expressed as:

$$\eta_{\text{EE}} = \frac{\tau}{P}$$

where τ is the system throughput, and P is the consumed power.

1.4 Imperfections

In real-world systems, several imperfections affect the performance of wireless communication systems. These imperfections include hardware impairments (HIs), such as non-linearities in amplifiers and phase noise in oscillators, as well as errors in channel estimation due to dynamic environments. This section discusses various imperfections, including imperfect channel state information and transceiver hardware impairments.

1.4.1 Imperfect channel state information

In practical wireless communication systems, obtaining perfect channel state information (CSI) is challenging, often leading to imperfect knowledge of the channel conditions between the transmitter and receiver. This imperfection, primarily due to channel estimation errors (CEE) and quantization errors, degrades system performance and efficiency.Recent studies also explore pilot contamination and training-based estimation strategies for massive MIMO and NOMA systems under imperfect CSI [4].

Channel estimation accuracy is affected by factors such as channel variability, estimation methods, and signal detection. An efficient estimation technique, like the minimum mean square error (MMSE) estimator, uses pilot symbols to reduce CEE. However, performance gains depend on optimal pilot patterns and estimation strategies, which require additional resources and are application-specific.

Under MMSE estimation [**?** **?**], the channel can be modeled as:

$$h_k = \hat{h}_k + \epsilon_k \tag{1.5}$$

where h_k is the actual channel, $\hat{h}_k$ is its estimate, and $\epsilon_k \sim \mathcal{CN}(0, \sigma_e^2)$ represents the estimation error, assumed to be a complex Gaussian random variable. Poor pilot design relative to coherence time and frequency can lead to an irreducible estimation error floor.

To mitigate the effects of imperfect CSI, robust resource allocation, improved channel estimation algorithms, feedback mechanisms, and resilient encoding/decoding techniques can be employed to enhance system performance.

1.4.2 HIs

In practical wireless systems, HIs such as phase noise and in-phase/quadrature (I/Q) imbalance degrade system performance. Although compensation algorithms can mitigate these effects, residual impairments persist. HIs cause discrepancies between the intended signal x and the transmitted or received signal, introducing distortion.

Taking HIs into account, the received signal can be modeled as:

$$y = \sqrt{P}h(x + \eta_t) + \eta_r + n \tag{1.6}$$

where P is the transmit power, $\eta_t \sim \mathcal{CN}(0, \kappa_t^2)$ and $\eta_r \sim \mathcal{CN}(0, \kappa_r^2 P|h|^2)$ represent distortion noise due to transmitter and receiver impairments, and $n \sim \mathcal{CN}(0, \sigma^2)$ is the additive white Gaussian noise. Parameters κ_t and κ_r (error vector magnitudes) quantify hardware imperfections.

The aggregate effect of transceiver HIs can be characterized by:

$$\kappa^2 = \kappa_t^2 + \kappa_r^2 \tag{1.7}$$

Substituting this into the signal model, the received signal becomes:

$$y = \sqrt{P}h(x + \eta) + n \tag{1.8}$$

where $\eta \sim \mathcal{CN}(0, \kappa^2)$ captures the total distortion.

1.5 Impulsive Noise

In practical wireless environments, the assumption of AWGN is often violated due to the presence of impulsive noise (Im-N). Impulsive noise is characterized by sudden, high-amplitude bursts of interference that occur unpredictably in time. Unlike AWGN, which has a continuous and low-power nature, Im-N can cause brief but significant disruptions in signal reception. These disturbances are typically generated by switching operations, electromagnetic discharges, or high-voltage equipment, and are prevalent in industrial areas, smart grids, urban networks, and indoor wireless settings.

Im-N severely degrades the performance of wireless communication systems, especially in dense and heterogeneous networks where multiple access technologies like NOMA are employed. NOMA relies on power-domain multiplexing and SIC, both of which are sensitive to noise-induced errors. When Im-N disrupts a low-power signal, it can cause SIC failures, leading to increased outage probability and reduced system reliability.

Given the critical impact of Im-N on network performance, its inclusion in the design and analysis of next-generation communication systems is essential. In the context of heterogeneous cellular NOMA networks, it becomes even more important to model and simulate real-world noise conditions accurately.

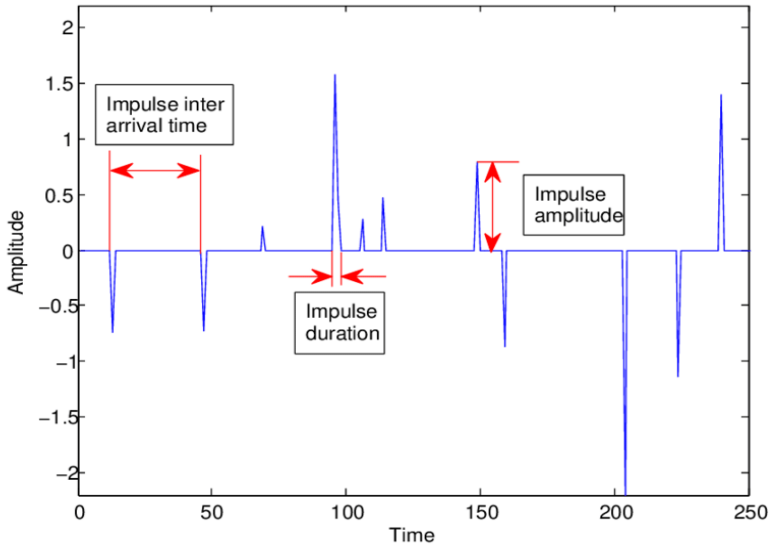

Figure 1.3: Characteristics of Impulsive Noise [5]

1.6 Motivation

The evolution toward 6G wireless networks demands communication systems that not only support ultra-dense deployments but also maintain high spectral efficiency, low latency, and robust energy performance. Among the prominent solutions addressing these demands is NOMA, particularly when integrated into Heterogeneous Cellular Networks (HCNs) that include both macro and low-power pico base stations. While extensive theoretical research has highlighted the benefits of NOMA, practical deployment in real-world environments necessitates performance evaluation under non-ideal operating conditions, which are often overlooked in conventional analysis.

One such practical challenge arises from Im-N, a highly disruptive form of interference that deviates from the classical Gaussian noise assumption. Found in industrial zones, power-line communications, and densely populated urban areas, Im-N can cause sporadic but intense interference that significantly degrades signal quality. Since NOMA is inherently sensitive to signal interference due to its reliance on SIC, the impact of Im-N on outage probability and energy efficiency becomes a critical area of investigation. The first study comprehensively analyzes this scenario, revealing how NOMA outperforms orthogonal multiple access (OMA) even in the presence of impulsive disturbances, and identifies system parameters that mitigate performance degradation.

In addition to environmental impairments, hardware imperfections and channel estimation errors are other inevitable practical limitations that affect real-world NOMA deployment. Transceiver distortions, quantified via HI, and i-CSI due to limited feedback and estimation inaccuracies, can lead to residual interference in SIC and degraded QoS. The second study focuses on quantifying the effect of HI and i-CSI within the HCN-NOMA framework. Using stochastic geometry for system modeling, it presents a realistic performance analysis, showing that while NOMA remains more efficient than OMA, its relative advantage depends heavily on system design choices, including power allocation and user pairing strategies under imperfect SIC.

Together, these two investigations reflect a holistic perspective on the practical challenges of NOMA deployment in future networks. By examining the performance of NOMA under both environmental (Im-N) and system-level (HI and i-CSI) impairments, they motivate the need for robust design strategies that can adapt to and compensate for these non-idealities. The combination of these studies forms a strong foundation for this thesis, which aims to contribute toward the development of realistic and resilient 6G wireless communication frameworks.

1.7 Thesis outline,Contributions

The report is divided into the following chapters:

- **Chapter 1** provides the *Introduction and Background* for the thesis. It outlines the motivation, objectives, contributions, and the necessary background related to NOMA in Heterogeneous Cellular Networks, setting the stage for the chapters that follow.

- **Chapter 2** discusses the *Performance Analysis of NOMA in HCN with HIs and i-CSI*. This chapter includes an introduction, system model, outage probability analysis, system throughput analysis, discussions on numerical and simulation results, and a summary.

- **Chapter 3** focuses on the *Performance of Heterogeneous Cellular NOMA Networks in Im-N*. It covers the introduction, system model, mathematical modeling of Im-N, outage probability analysis, system throughput analysis,

energy efficiency analysis, bar plot analysis, numerical and simulation results, and concludes with a summary.

- **Chapter 4** presents the *Conclusions and Future Works*. All the contributions of the thesis are summarized in this chapter, along with key insights and conclusions. Additionally, the scope for future research directions is discussed.

While this chapter establishes the foundational concepts of NOMA, wireless channel modeling, and the significance of imperfections in real-world communication systems, it does not quantify their effects in a practical setting. The next chapter addresses this gap by performing a detailed performance analysis of NOMA in HCNs under HIs and i-CSI conditions, thus translating theoretical insights into measurable system behavior.

CHAPTER 2

PERFORMANCE ANALYSIS OF NOMA IN HCN WITH HARDWARE IMPAIREMENTS AND IMPERFECT CSI

In this chapter, a detailed analysis of NOMA performance in HCN is carried out, taking into account practical limitations such as HIs and i-CSI. The goal is to evaluate the reliability and throughput of the system under these non-ideal conditions. Various analytical expressions are derived and supported with numerical and simulation results. In a multi-tier HCN with MBS and PBS, NOMA is used to boost spectral efficiency and achieve higher data rates in the sixth-generation wireless networks. This study investigates HCN-NOMA performance under the practical consideration of i-CSI using stochastic geometry. The study compares OMA and NOMA, evaluating outage probability, and system throughput for both perfect and i-SIC scenarios in multi-tier HCN. Despite HIs and i-CSI in NOMA, noticeable performance improvements of up to 57% are observed.

2.1 Introduction

[7] Ultra-dense networks (UDNs) with small cells are emerging as a solution in 6G technology research to address challenges in user coverage, data rates requirement, lower latency, and energy consumption [8]. Allocating dedicated time slots and frequency bands in UDNs is impractical, especially with low data rate requirements or poor channel conditions. Therefore, NOMA enables multiple users to share the same frequency band simultaneously with distinct power levels, offering a viable solution for future UDNs [9]. SIC enhances QoS by prioritizing decoding signals from weaker users, improving data rates, and reducing error rates for users facing poor channel conditions [10]. To address the requirements of high user density

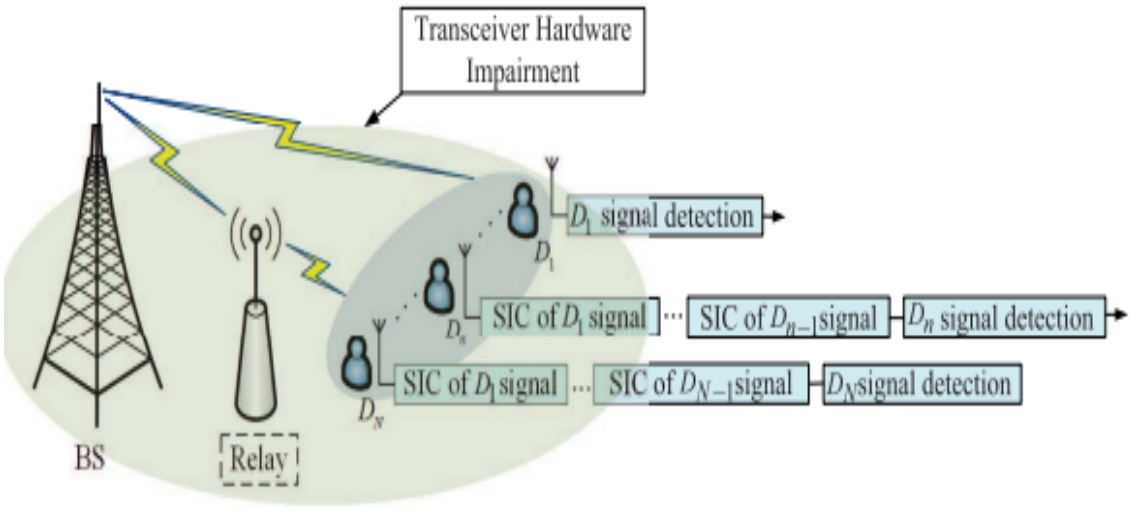

Figure 2.1: Illustration of multiuser NOMA networks [6].

and increased data rates, NOMA is integrated into low-power PBS to configure a HCN-NOMA. A unmanned aerial vehicle (UAV)-assisted HCN combines NOMA-based aerial and mmWave terrestrial base stations, showcasing NOMA's superior outage performance and ergodic sum rate with optimized power coefficients and data rates for randomly deployed users [11]. The performance of power beacon-assisted cooperative-NOMA (Co-NOMA) in wireless powered communication HCN was assessed incorporating a realistic non-linear energy harvesting model [12], while study in [13], and [14] examines the application of simultaneous wireless information and power transfer (SWIPT) in NOMA and Co-NOMA in HCN networks with randomly distributed users, but relied on ideal assumptions of HIs and CSI, which is not possible in practice. The study analyzes NOMA with i-SIC in a multi-relay energy harvesting system [15], and impact of non-linear distortions by high power amplifier in HCN-NOMA with i-SIC but with perfect CSI [16]. A hybrid NOMA-OMA framework is proposed, optimizing power allocation and channel overlap for users to enhance spectral efficiency under i-SIC and i-CSI constraints, aiming to maximize sum-rate throughput [17]

This study investigates the integration of NOMA into HCN using the PPP under the scenarios of i-SIC and i-CSI, an aspect that, to the authors' knowledge, has not been thoroughly explored in the existing literature. The manuscript presents several noteworthy contributions, detailed as follows:

- Considering the mathematical tractability and spatial consistency offered by

the PPP for wireless networks, we utilized PPP within the HCN to spatial distributions of both MBS and PBS.

- This study compares HCN-NOMA and OMA systems, focusing on user performance under HI. The analysis includes deriving closed-form expressions for outage probabilities in scenarios with both perfect and i-CSI.
- Exploring the interplay between HI and i-CSI unveils valuable insights into their collective impact on system performance and dynamics. Graphical representations clarify OP and SE, enriching the quantitative analysis.

2.2 System Model

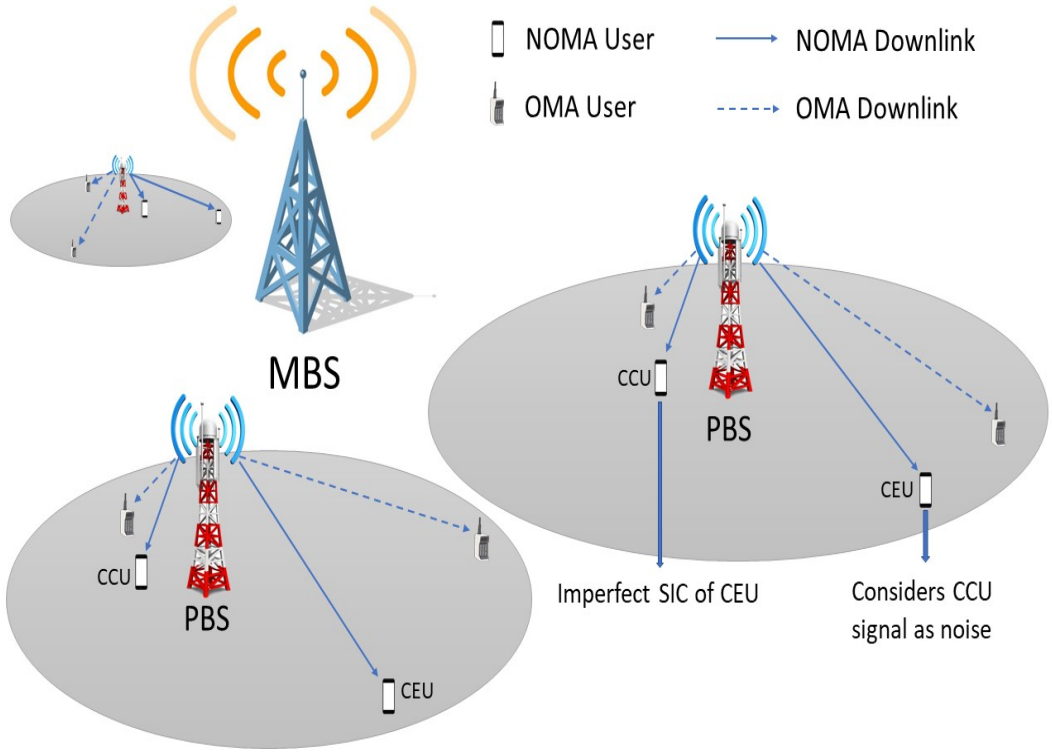

Figure 2.2: Downlink NOMA model with one MBS and multiple PBS along with NOMA paired users

A two-tier HCN, integrating NOMA with MBS and NOMA-enabled PBS enhances system flexibility, accommodating users with distinct channel conditions and diverse QoS requirements in the shared downlink spectrum. PPP is utilized in HCN for the mathematical modeling of MBS and PBS distributions, offering a spatially realistic framework for wireless network performance evaluation and system design. Nodes and BSs are independently distributed using PPP (Ω_t, λ_t) for tiers

($t \in \{m, p\}$), and users are distributed via PPP Ω_u with density λ_u. Each node has a single antenna and operates in half-duplex mode. In NOMA, a_n signifies the power coefficients for the n-th user, $\mathcal{Y}_t$, and P_t denotes coverage range and transmit power for the t-th tier, respectively.

The connectivity between a MBS and a macro-based user (MU) adheres to the nearest neighbor connection policy. A bounded path loss model denoted by $P(r) = \frac{1}{1+r_t^{\nu_t}}$ [18] is considered. The path loss exponent for the t-th tier is denoted by ν_t, with r_t representing the distance between the serving BS and the typical user. Consequently, $|h_t|^2 = |\tilde{h}_t|^2 P(r)$ defines the total channel gain experienced by the selected user in the t-th tier, where $\tilde{h}_t \sim \mathcal{CN}(0, 1)$. The system-wide transmission bandwidth is set at 1 Hz, and R denotes the desired data rate for the specific user.

This study considers i-CSI, arising from real-world factors like channel estimation errors. Due to the PBS tier's limited backhaul capacity compared to the MBS tier, minimizing CSI estimation and feedback overhead is crucial. Hence, our analysis focuses specifically on the impact of channel estimation errors at the PBS tier in the system model. The CSI at all nodes is determined using MMSE-based estimator, with the estimated CSI's relationship to actual channel coefficients discussed in [15], denoted as $h_{t,i} = \hat{h}_{t,i} + e_i$, where e_i is the channel estimation error for i-th user, modeled as $e_i \sim \mathcal{CN}(0, \sigma_e^2)$ and $\hat{h}_{t,i}$ is the estimate of the $h_{t,i}$. Thus, the estimate $\hat{h}_{t,i}$ follows complex Gaussian distribution with zero mean and variance $\left(1 + r_{t,i}^{\nu_t}\right)^{-1} - \sigma_e^2$. **Note:** The $\tilde{h}_t$ represents the actual complex Gaussian distributed channel, where $|\hat{h}|^2$ and $|\hat{\tilde{h}}|^2$ denotes estimated ordered and estimated unordered channel gains, respectively.

2.3 Mathematical analysis

2.3.1 PBS User's SINR (i-CSI, excluding NOMA)

Mathematical expression of the signal transmitted from the PBS is denoted as $X_{p,tx} = x_p\sqrt{P_p}$, while the signal received at the specific user linked to PBS (PU) is represented as

$$X_{p,rx} = (x_p + \eta_{si})\sqrt{P_p}\left(\hat{\ddot{h}}_{p_o} + e_p\right) + \underbrace{\sum_{t\in(m,p)} x_t\sqrt{P_t}\sum_{r\in\Omega_t\setminus\{p_o\}} \ddot{h}_r}_{\text{Intra-tier and Inter-tier interference by BSs}} + \eta_{dj} + n_p, \tag{2.1}$$

where $\eta_{si} \sim \mathcal{CN}(0, \kappa_{si}^2)$ and $\eta_{dj} \sim \mathcal{CN}\left(0, \kappa_{dj}^2 P_i|\hat{\ddot{h}}_{p_o}|^2\right)$ denote distortion noises arising due to impairments of the transmitter and receiver, respectively. The parameters $k_{si}^2 \geq 0$ and $k_{dj}^2 \geq 0$ signify the level of impairment and can be termed as error vector magnitudes (EVMs). Here, EVM measures standard of RF transceiver and can be defined as the ratio of average distortion magnitude to the average signal magnitude. Aggregate distortion noise power at PU can be obtained from (2.1), as

$$E\{|P_p\hat{\ddot{h}}_{p_o}\eta_{si} + \eta_{dj}|^2\} = P_p|\hat{\ddot{h}}_{p_o}|^2\left(\kappa_{si}^2 + \kappa_{dj}^2\right). \tag{2.2}$$

By using (2.2), we can express (2.1) as

$$X_{p,\mathrm{rx}} = (x_p + \eta_{ij})\sqrt{P_p}\left(\hat{\ddot{h}}_{p_o} + e_p\right) + \sum x_t\sqrt{P_t}\sum \ddot{h}_r + n_p \tag{2.3}$$

where $\eta_{ij} \sim \mathcal{CN}(0, \kappa^2)$ denotes distortion noise due to transceiver hardware impairments (HIs) and $\kappa = \sqrt{\kappa_{si}^2 + \kappa_{dj}^2}$. We consider that all the nodes have the same HIs for IP. Here, for $k = 0$ (ideal hardware case).

where x_p represents the desired signal for the PU, $\hat{\ddot{h}}_j$ is the estimated unordered channel coefficient to the specific PU from the j-th BS ($j \in \{p_o, r\}$), while n_p denotes the channel noise. The SINR at a selected PU can be expressed as [**?**]

$$\gamma_p = \frac{\rho_p P_p|\hat{\ddot{h}}_{p_o}|^2}{\sum_t \rho_t'\mathbb{I}_t + \rho_p\sigma_e^2\left(1+\kappa^2\right) + \rho_p|\hat{\ddot{h}}_{p_o}|^2k^2 + 1}, \tag{2.4}$$

where ρ_p is the transmit SNR at the PBS tier and is determined as $\rho_p = \mathbb{E}\left[x_p^2\right]/\sigma_p^2$ where σ_p^2 is the noise variance. $\rho_t' = P_t/\sigma_p^2$ denotes the transmit SNR from the t-th tier, which interferes with the selected PU. Without loss of generality, if the selected PU is situated at the point of origin and the designated PBS is positioned at p_o, according to Slivnyak's theorem [19], $\rho_p'\mathbb{I}_p$ denotes the intra-tier interference caused by the PBS tier on the PU. In this case, $\mathbb{I}_p = \sum_{j\in\Omega_p\setminus\{p_o\}}|\ddot{h}_j|^2$, where $|\ddot{h}_j|^2$ is the overall channel gain from the j-th PBS to the selected PU. Likewise, $\rho_m'\mathbb{I}_m$ denotes

inter-tier interference originating from the MBS tier towards the selected PU. In such case, $\mathbb{I}_m = \sum_{i\in\Omega_m} |\ddot{h}_i|^2$, where $|\ddot{h}_i|^2$ represents the total channel gain for the selected PU from the i-th transmitter of the MBS tier.

2.3.2 PBS User's SINR (i-CSI, NOMA with i-SIC)

The power domain NOMA is applied by the PBS to cater M_p users, where the power allocation factors $a_1 \geq \cdots \geq a_{M_p}$ are determined according to the sorted channel gains $|h_1^{p_o}|^2 \leq \cdots \leq |h_{M_p}^{p_o}|^2$ of the NOMA users. In this context, a 'near user' or 'cell center user (CCU)' is defined by having a strong channel gain, whereas a 'far user' or 'cell edge user (CEU)' has a weaker channel gain. Assuming uniform signal power for all NOMA users, the i-th NOMA user's intended signal is expressed as x_i, while the transmitted signal by the PBS is represented by $X_{p,tx} = \sum_{i=1}^{M_p} x_i\sqrt{a_i P_p}$. The signal received by the k-th user is expressed as

$$X_{k,rx}^{p} = \left(\hat{h}_k^{p_o} + e_k\right)(s_k + \eta_{ij})\sqrt{P_p} + \underbrace{\sum_{t\in(m,p)} x_t\sqrt{P_t}\sum_{r\in\Omega_t\setminus\{p_o\}} h_r}_{\text{Intra-tier and Inter-tier interference by BSs}} + n_k, \tag{2.5}$$

where s_k comprises of

$$s_k = \sqrt{a_k}x_k + \underbrace{\sum_{u=1}^{k-1}\sqrt{\beta_u}\sqrt{a_u}x_u}_{\text{i-SIC}} + \underbrace{\sum_{u=k+1}^{M_p}\sqrt{a_u}x_u}_{\text{Inter-User Interference}} \quad . \tag{2.6}$$

In the downlink scenario of i-SIC, the high SNR signal is not entirely decoded by users of superior channel conditions, resulting in incorrect subtraction from the NOMA signal transmitted by the BS. Consequently, users with favorable channel conditions experience interference in the decoding process due to the remaining high SNR message residual signal component. The k-th user performs SIC by decoding the message of the j-th user; thus, the SINR at the k-th user, where $j \leq k$, is denoted as

$$\gamma_{j\to k}^{p} = \frac{\rho_p P_p a_j \left|\hat{h}_k^{p_o}\right|^2}{\rho_p P_p \left|\hat{h}_k^{p_o}\right|^2 \left(\sum_{n=j+1}^{M_p} a_n + \kappa^2\right) + \sum_t \rho_t^i \mathbb{I}_t + \rho_p\sigma_e^2\left(1+\kappa^2\right) + 1}. \tag{2.7}$$

and a_n is the power allocation factor for users indexed by $n \in \{k, j\}$. Residual interference from i-SIC at different users, denoted by $\beta_n = \beta; \forall \{n \in (1, 2, ..., M_p - 1)\}$, retains β fraction of high SNR symbols in the superposed NOMA signal such that $0 \leq \beta \leq 1$. Thus, $\beta = 0$ signifies perfect SIC with no residues, while $\beta = 1$ implies no SIC. The user at the maximum distance from the BS remains uninfluenced by i-SIC, as it does not engage in SIC, treating signals from other users as noise. Expressing the SINR for the k-th user decoding its own message as

$$\gamma_k^p = \frac{\rho_p P_p a_k \left|\hat{h}_k^{p_o}\right|^2}{\rho_p P_p \left|\hat{h}_k^{p_o}\right|^2 \left(\sum_{n=k+1}^{M_p} a_n + \kappa^2\right) + \sum_t \rho_t^i \mathbb{I}_t + \rho_p \sigma_e^2 (1 + \kappa^2) + 1}. \tag{2.8}$$

2.4 Outage analysis

In this section, the rate OP is assessed across various tiers. Generally, Outage Probability quantifies the likelihood of significant performance degradation in a wireless communication link, including signal strength reduction, data rate decline, or increased error rate.

2.4.1 Outage Analysis for PBS Tier with i-CSI & HI (w/o NOMA)

The rate OP at a typical PU is determined by considering a uniform distance from the PBS, is given by

$$\begin{aligned} \mathbb{P}_O^p &= \Pr\left[W_p \times \log_2(1 + \gamma_p) < R\right], \\ &= \Pr\left[|\hat{\tilde{h}}_{p_o}|^2 < \frac{\phi_p}{\rho_p P_p}\left(1 + \rho_p \sigma_e^2 \left(1 + \kappa^2\right) + \sum_t \rho_t^i \mathbb{I}_t\right)\right], \end{aligned} \tag{2.9}$$

where, W_p represents the bandwidth assigned to OMA-based PU, and γ_p denotes the SINR at PU, as defined in (2.4), and R indicates the user's desired data rate. Consequently, the SINR threshold is defined as $\phi = 2^{2R} - 1$. Assuming a homogeneous PPP and utilizing polar coordinates, the CDF of the unordered channel gain in the PBS tier is formulated as [20]:

$$F_{\left|\hat{\tilde{h}}_{p_o}\right|^2}(y) = \frac{2}{\mathcal{Y}_p^2} \int_0^{\mathcal{Y}_p} (1 - e^{-\left(\frac{1}{1 + r_p^{\nu_p}} + \sigma_e^2\right)^{-1} y}) r_p dr_p. \tag{2.10}$$

By applying the G-C quadrature [20] to (2.10), we get

$$F_{\left|\hat{\tilde{h}}_{p_o}\right|^2}(y) \simeq \sum_{q=0}^{Q} b_q^p e^{-\frac{c_q^p}{1+c_q^p\sigma_e^2}y}, \tag{2.11}$$

Thus, the OP, as expressed in (2.9), can be reformulated as,

$$\begin{aligned}\mathbb{P}_O^p &\approx \sum_{q=0}^{Q} b_q^p e^{-\frac{c_q^p}{1+c_q^p\sigma_e^2}\left\{\frac{\phi_p}{\rho_p P_p}\left(1+\rho_p\sigma_e^2\left(1+\kappa^2\right)+\sum_t \rho_t^i\mathbb{I}_t\right)\right\}},\\ &\approx \sum_{q=0}^{Q} b_q^p e^{-\frac{c_q^p\phi_p}{\rho_p P_p\left(1+c_q^p\sigma_e^2\right)}\left(1+\rho_p\sigma_e^2\left(1+\kappa^2\right)\right)} \prod_t \mathcal{L}_{\mathbb{I}_t}(\rho_t^i s_p).\end{aligned} \tag{2.12}$$

where Q strikes a balance between accuracy and complexity, $b_q^p = -w_Q\sqrt{1-\theta_q^2}\left(\frac{1}{2}\left(\theta_q+1\right)\right)$, $w_Q = \frac{\pi}{Q}$, $\theta_q = \cos\left(\frac{2q-1}{2Q}\pi\right)$, $b_0 = -\sum_{q=1}^{Q} b_q^p$, $c_q^p = 1+\left(\frac{\mathcal{Y}_p}{2}\theta_q+\frac{\mathcal{Y}_p}{2}\right)_p^{\nu}$, $c_0 = 0$, and $s_p = \frac{c_q^p\phi_p}{\rho_p P_p\left(1+c_q^p\sigma_e^2\right)}$.

Laplace transform (LT) of interference from the t-th tier is $\mathcal{L}_{\mathbb{I}_t}(s)$ expressed [18] as

$$\mathcal{L}_{\mathbb{I}_t}(s) = e^{\pi\lambda_t(s^{\mu_t}\Gamma(1-\mu_t,s)-s^{\mu_t}\Gamma(1-\mu_t))}, \tag{2.13}$$

where $\mu_t = 2/\nu_t$, $\Gamma(z) = \int_0^\infty x^{z-1}e^{-x}dx$ and $\Gamma(z,x) = \int_x^\infty t^{z-1}e^{-t}dt$.

2.4.2 Outage Analysis for PBS Tier (NOMA with HI & i-CSI)

We examine a scenario where the user's QoS requirements specify a predefined target data rate R, leading to the formulation of the OP as follows:

$$\mathbb{P}_k^{O,p} = \Pr\left[\gamma_k^{p,i-SIC} < \phi_k, \gamma_{j\to k}^{p,i-SIC} < \phi_j\right], \tag{2.14}$$

where $\gamma_{j\to k}^{p,i-SIC}$ and $\gamma_k^{p,i-SIC}$ are given in (2.7), and (2.8) respectively. As the successful self-message decoding in SIC directly impacts the OP, it can be expressed for the k-th user as:

$$\mathbb{P}_k^{O,p} = \Pr\left[|\hat{h}_k^{p_o}|^2 < \frac{\psi_{max,i-S}^{i-C}(1+\rho_p\sigma_e^2\left(1+\kappa^2\right)+\sum_t \rho_t^i\mathbb{I}_t)}{\rho_p P_p}\right]. \tag{2.15}$$

This results in the OP as

$$\mathbb{P}_k^{O,p} = F_{\left|\hat{h}_k^{p_o}\right|^2}(y), \tag{2.16}$$

where $y = \frac{\psi^{i-C}_{max,i-S}(1+\rho_p\sigma_e^2\left(1+\kappa^2\right)+\sum_t \rho_t^i \mathbb{I}_t)}{\rho_p P_p}$ and $\psi^{i-C}_{max,i-S} = \max\left(\psi^{i-C}_{(1,i-S)}, \psi^{i-C}_{(2,i-S)}, \ldots, \psi^{i-C}_{(k,i-S)}\right)$. For a user with $k = 1$, OP is simply calculated with $y = \frac{\psi^{i-C}_{j,i-S}(1+\rho_p\sigma_e^2\left(1+\kappa^2\right)+\sum_t \rho_t^i \mathbb{I}_t)}{\rho_p P_p}$, as it decodes its own message without performing SIC. $\psi^{i-C}_{j,i-S} = \frac{\phi_j}{a_j - \phi_j\left(\sum_{l=j+1}^{M_p} a_l + \kappa^2\right)}$, where, ϕ_j is defined as $2^{R_j} - 1$, with R_j representing the target data rate for the j-th user.

The connection between the ordered and unordered channel gains of the PBS tier, taking into account i-CSI denoted as $F_{\left|\hat{\hat{h}}_{p_o}\right|^2}(y)$, is expressed as follows [20]:

$$F_{\left|\hat{h}_k^{p_o}\right|^2}(y) = \epsilon_k \sum_{d=0}^{M_p-k} \binom{M_p-k}{d} \frac{(-1)^d}{k+d} \left(F_{\left|\hat{\hat{h}}_{p_o}\right|^2}(y)\right)^{k+d}. \tag{2.17}$$

Upon substituting (3.13) in (3.18) and employing the multinomial theorem, the CDF for the ordered channel gains is obtained as

$$\begin{aligned} F_{\left|\hat{h}_k^{p_o}\right|^2}(y) \simeq & \epsilon_k \sum_{d=0}^{M_p-k} \binom{M_p-k}{d} \frac{(-1)^d}{k+d} \sum_{T_k^d} \binom{k+d}{l_0+\ldots+l_N} \\ & \times \left(\prod_{q=0}^{Q} (b_q^p)^{l_q}\right) e^{-\sum_{q=0}^{Q} l_q \frac{c_q^p}{1+c_q^p\sigma_e^2} y}. \end{aligned} \tag{2.18}$$

Given the uniform distance from the PBS and considering the ordered channel gains, the rate OP at the k-th selected PU is given by

$$\begin{aligned} \mathbb{P}_k^{O,p} \approx & \epsilon_k \sum_{d=0}^{M_p-k} \binom{M_p-k}{d} \frac{(-1)^d}{k+d} \sum_{T_k^d} \binom{k+d}{l_0+\ldots+l_N} \prod_{q=0}^{Q} (b_q^p)^{l_q} \\ & \times e^{-\sum_{q=0}^{Q} l_q \frac{c_q^p \psi^{i-C}_{\max,i-S}}{\rho_p P_p (1+c_q^p\sigma_e^2)}\left(1+\rho_p\sigma_e^2\right)} \prod_t \mathcal{L}_{\mathbb{I}_t}(\rho_t^i s_p), \end{aligned} \tag{2.19}$$

where $\epsilon_k = \frac{M_p!}{(k-1)!(M_p-k)!}$, $s_p = \frac{\psi^{i-C}_{\max,i-S}\sum_{q=0}^{Q} l_q \frac{c_q^p}{1+c_q^p\sigma_e^2}}{\rho_p P_p}$, $T_k^d = \left\{(l_0,\ldots,l_N) | \sum_{i=0}^{N} l_i = k+d\right\}$, and $\binom{k+d}{l_0+\ldots+l_N} = \frac{(k+d)!}{l_0!\ldots l_N!}$.

Observably, the user with $k = 1$ does not engage in SIC, hence the term $\psi^{i-C}_{\max,i-S} = \psi^{i-C}_{1,i-S}$.

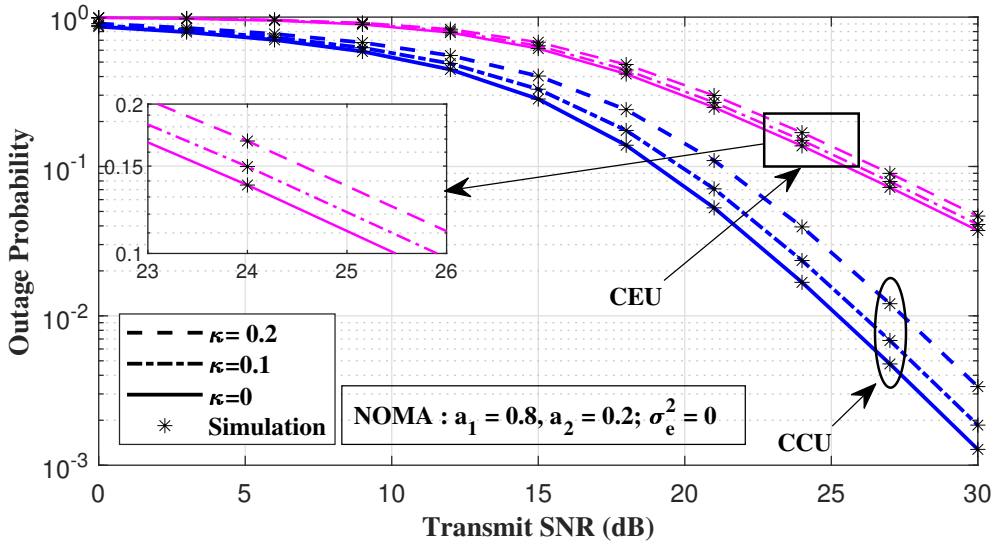

Figure 2.3: OP for varying HI parameter values utilizing NOMA

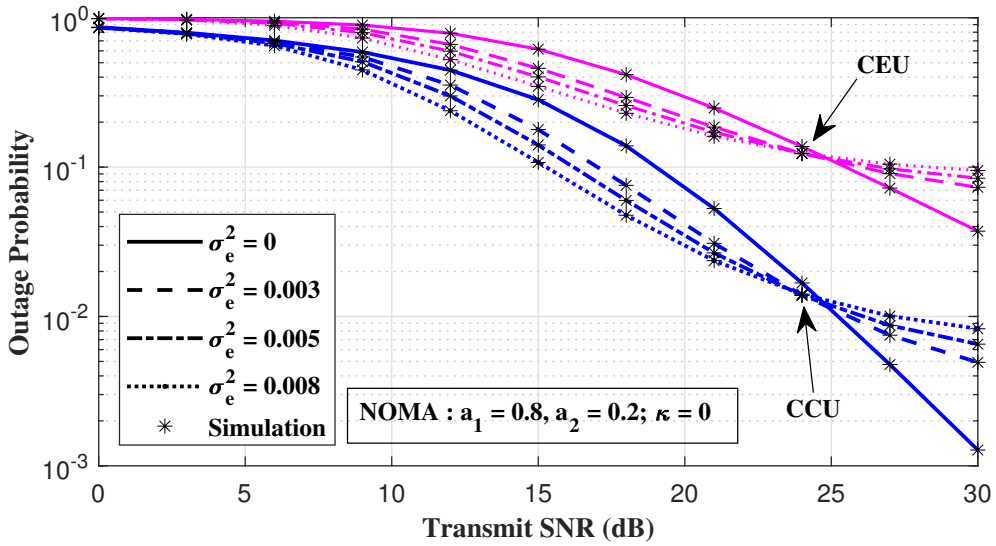

Figure 2.4: OP across multiple i-CSI parameter values utilizing NOMA

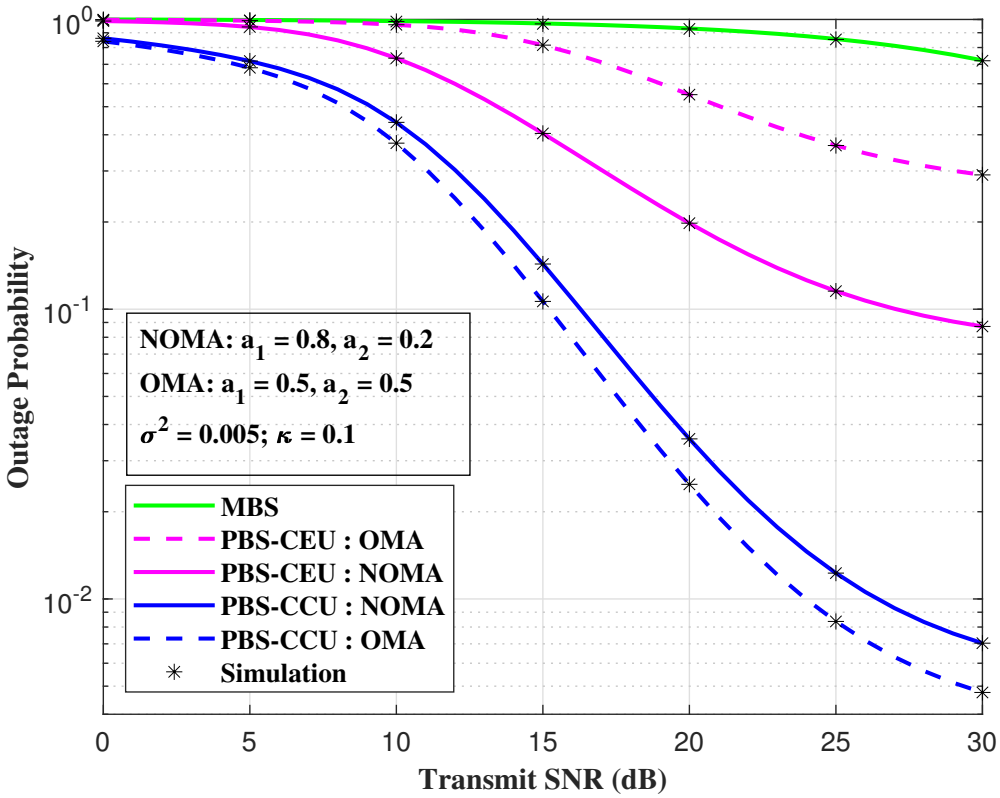

Figure 2.5: Impact of HI and i-CSI for both OMA and NOMA

2.5 System Throughput analysis

In this section, we analyze the system throughput performance of the considered NOMA-enabled HCN under practical impairments such as hardware non-linearities and i-CSI. The system throughput is an essential metric that measures the effective data rate achieved by successfully served users per unit bandwidth. It captures the impact of various imperfections and outage events on the overall system efficiency.

The system throughput, denoted by τ_{sys} (in bps/Hz), can be expressed as:

$$\tau_{\text{sys}} = \left(1 - P_{\text{O},p}^{\text{CEU}}\right) R_1 + \left(1 - P_{\text{O},p}^{\text{CCU}}\right) R_2, \tag{2.20}$$

where $P_{\text{O},p}^{\text{CEU}}$ and $P_{\text{O},p}^{\text{CCU}}$ represent the outage probabilities of the cell-edge user (CEU) and the cell-center user (CCU), respectively. R_1 and R_2 denote the target data rates for the CEU and CCU. This formulation highlights that the system throughput depends not only on the achievable data rates but also on the reliability of the communication links under the impact of practical impairments.

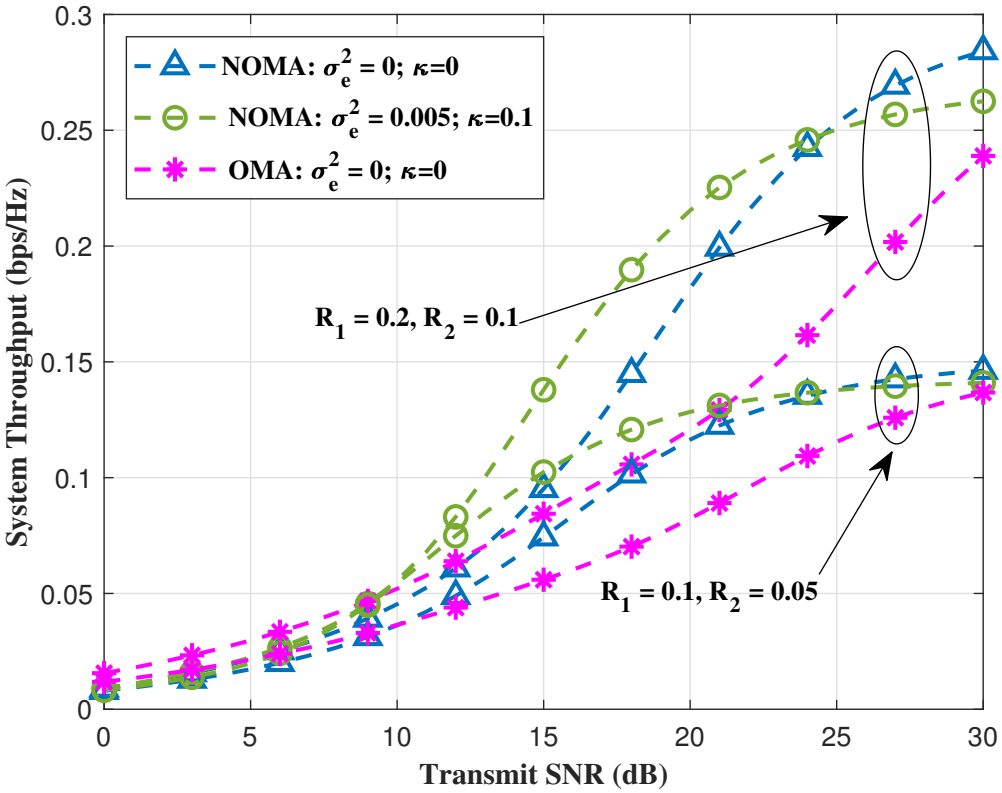

Figure 2.6: SE in HCN for OMA and NOMA under HI and i-CSI

2.6 Discussions on numerical and simulation results

In this section, inference are drawn based on the simulation results on the OP, from which system throughput is derived. The analytical results are validated using simulations, with parameters including MBS transmitting power (P_m) set at 40 W and PBS transmitting power (P_p) at 1 W, with MBS node density (λ_m) at $5 \times 10^{-5}\text{m}^{-2}$, PBS node density ($\lambda_p$) at 10^{-4}m^{-2}, and user node density (λ_u) at $5 \times 10^{-4}\text{m}^{-2}$. Power allocation coefficients for NOMA users (a_k) are 0.8 and 0.2. Coverage ranges are set to 1000 m for MBS ($\mathcal{Y}_m$) and 5 m for PBS ($\mathcal{Y}_p$), with path loss exponents of 3 for MBS (ν_m) and 4 for PBS (ν_p). Target data rates for CEU (R_1) and CCU (R_2) are specified as 0.1 bps and 0.05 bps, respectively. The channel estimation error variance (σ_e^2) is set to 0.005, similar to the ones used by [16], [21], and [20].

2.6.1 Simulation Parameters

Table 2.1: Simulation Parameters

Parameters	**Symbols**	**Value**
Transmitting power from MBS, and PBS	P_m, P_p	40 W, 1 W
MBS, PBS, and user's density	λ_m, λ_p, λ_u	$5 \times 10^{-5}m^{-2}$, $10^{-4}m^{-2}$, $5 \times 10^{-4}m^{-2}$
Power allocation coefficients for NOMA	a_k	$0.8, 0.2$
Coverage range of MBS, PBS	$\mathcal{Y}_m, \mathcal{Y}_p$	1000 m, 5 m
Path loss exponent for MBS, PBS	ν_m, ν_p	$3, 4$
Target data rate (CEU, CCU)	R_1, R_2	$0.1, 0.05$
Hardware Impairement coefficient	κ	0.1
Channel estimation error variance	σ_e^2	0.005

2.6.2 Numerical Results

The outage performance of the HCN-NOMA system for the PBS tier, considering two users, is depicted in Fig. 2.3. In this figure, the OP is plotted across various HI parameter values in NOMA. The analysis reveals a significant degradation in the outage performance for both CEU and CCU due to HIs. Specifically, the CCU experiences performance improvements of approximately 1.38 dB and 2.21 dB when the HI parameters are reduced from 0.2 to 0.1 and then to 0, respectively, achieving an outage probability of 10^{-2}.

In Fig. 2.4, the OP is plotted against various i-CSI parameter values in NOMA.

The figure illustrates that outage performance enhances as the SNR increases, reaching its peak at high SNRs (around 30 dB), beyond which an error floor is encountered. The NOMA system supports both CEU and CCU, with their respective power coefficients clearly indicated in the plot. Interestingly, the outage performance shows distinct variations based on i-CSI coefficients for CCU and CEU, with significant improvements observed at low SNRs ($\leq$ 25 dB). However, as the SNR continues to rise, the performance degrades at higher SNR levels when i-CSI is increased.

Fig. 2.5 illustrates a comparative analysis between NOMA and OMA under the influence of HI and i-CSI within an HCN. The performance of users served by the PBS, categorized as CCU and CEU, is significantly better than those served by the MU. Specifically, within the PBS tier, the CCU consistently outperforms the CEU across various access schemes. NOMA demonstrates a clear performance advantage for CEUs, while OMAs are more beneficial for CCUs when specific power allocation coefficients are applied, highlighting the importance of signal power distribution. Despite OMA allocating equal power to both CEU and CCU, NOMA achieves superior overall performance primarily due to the increased power allocation to the CEU.

System throughput (bps/Hz) is calculated as $\tau_{sys} = \left(1 - \mathbb{P}_{CEU}^{O,p}\right) R_1 + \left(1 - \mathbb{P}_{CCU}^{O,p}\right) R_2$, where the OP at the PBS tier for the CEU, and CCU, denoted as $\mathbb{P}_{CEU}^{O,p}$ and $\mathbb{P}_{CCU}^{O,p}$ respectively, are determined by operating (2.19) at $k = 1$ and $k = 2$, with R_1 and R_2 denoting the target data rate for the CEU and CCU, as per [21], and [18]. Fig. 2.6 presents a comparative SE analysis for systems employing OMA and NOMA. The performance comparison includes both ideal systems and those with i-CSI and HI for NOMA. The study shows that increasing signal power significantly improves the outage performance of CCUs more than it adversely impacts the performance of CEUs. This results in superior system performance and higher throughput for NOMA compared to OMA. Additionally, i-CSI enhances system throughput, particularly in the low SNR region below 25 dB; however, NOMA and OMA experience performance degradation at high SNR levels. Despite overall system throughput decline with i-CSI in NOMA, NOMA's spectral efficiency under i-SIC surpasses OMA across the entire SNR range.

2.7 Summary

This study examines the impact of HI and i-CSI on the downlink performance of NOMA and OMA. It highlights notable effects on outage performance and system throughput within the HCN-NOMA system across different SNRs. Numerical results indicate that NOMA consistently outperforms OMA, especially under i-CSI conditions. By comparing ideal NOMA versus ideal OMA and NOMA with i-CSI versus OMA with i-CSI under the influence of HI, it is evident that NOMA offers superior spectral efficiency gains across a wide SNR range. Consequently, NOMA is identified as the preferred choice for realistic environments.

This chapter comprehensively analyzes the effects of HIs and i-CSI on NOMA performance within HCNs. However, it assumes an AWGN environment, which does not account for more disruptive real-world interference such as Im-N. The next chapter extends this work by evaluating the robustness of NOMA under Im-N scenarios, further pushing the boundary of practical feasibility analysis.

CHAPTER 3

ON PERFORMANCE OF HETEROGENEOUS CELLULAR NOMA NETWORKS IN IMPULSIVE NOISE

In this chapter, investigates the performance of multi-tier HCNs with MBS, PBS employing NOMA to improve SE and achieve higher data rates for the 6G wireless networks. Deployment in smart homes, grids, and industrial IoT is challenged by impulsive electromagnetic interference, rendering Gaussian noise-based analyses inadequate. Thus, this study uses stochastic geometry to compare HCN-NOMA performance under AWGN and Im-N, highlighting variations in system behavior. A comparative analysis of OMA and NOMA under these noise conditions is provided using metrics such as OP, throughput, and energy efficiency. Finally, results reveal NOMA's superior performance over OMA even in the presence of Im-N, identifying specific SNR ranges where NOMA's gains are maximized in both AWGN and Im-N scenarios.

3.1 Introduction

In 6G, UDNs are emerging as a key solution to enhance coverage, data rates, lower latency, and energy consumption [22]. Allocating dedicated resources (e.g. time-slots, and frequency-bands) in UDNs becomes challenging with low data rates requirements or poor channels conditions. NOMA enables efficient resource sharing for future UDNs [23], and its integration into HCNs with low-power PBS provides a scalable solution to meet the demands of high user density and data rates [24]. Additionally, the performance of cooperative NOMA in wireless-powered HCNs has

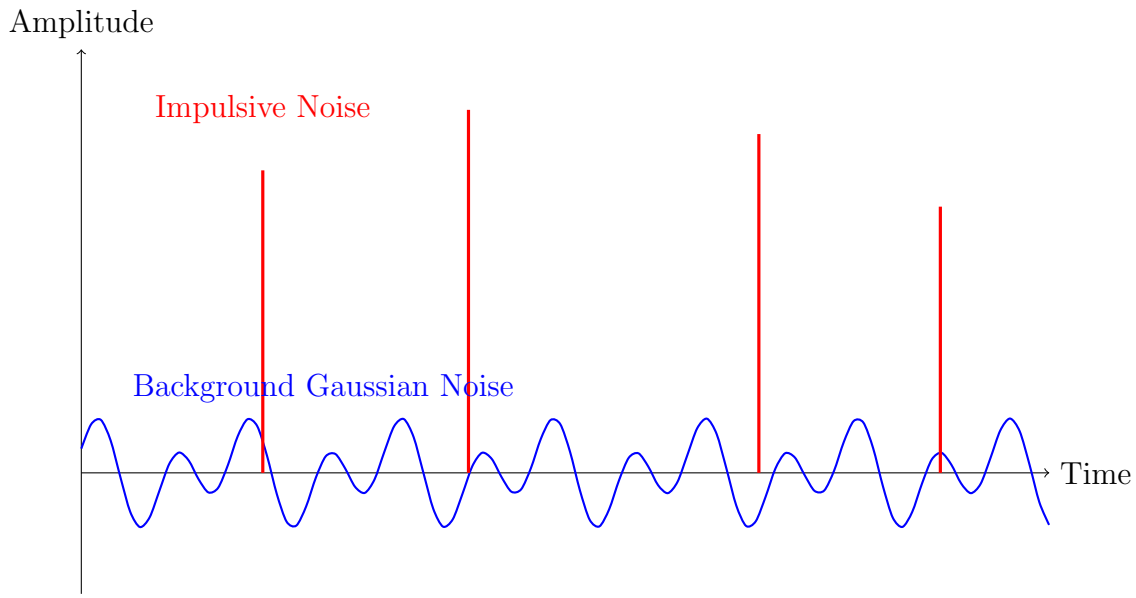

Figure 3.1: Illustration of impulsive noise superimposed on background Gaussian noise.

been evaluated, incorporating SWIPT for randomly distributed users [25]. An UAV-assisted HCN combines NOMA-based aerial and mmWave terrestrial base stations, showcasing NOMA's superior outage performance and ergodic sum rate with optimized power coefficients and data rates for randomly deployed users [26]. The authors in [27] investigates NOMA with i-SIC, focusing on the impact of non-linear distortions caused by high-power amplifiers in HCN-NOMA. Most research on NOMA systems assumes receivers are impaired by additive Gaussian noise, supported by the central limit theorem for mathematical simplicity and signal distribution. However, in practical scenarios, Im-N is common, particularly in environments like urban areas, manufacturing plants [28], power line communications [29], and indoor wireless networks [30], where factors like switching operations and partial discharge in high-voltage equipment create significant interference. Despite their usefulness, studies in [25]-[27] primarily focus on systems operating under AWGN. However, research indicates that systems designed for AWGN often suffer significant performance degradation in Im-N environments, and since power domain NOMA is particularly sensitive to such disturbances and variations in the amplitude, studying NOMA under fading and Im-N is essential for defining practical system limits and design. To address this challenge, recent studies have shifted focus toward analyzing NOMA performance under fading and Im-N environments [31]. Hence, this motivates investigating NOMA integration into HCN using the PPP under Im-N, offering a comparative

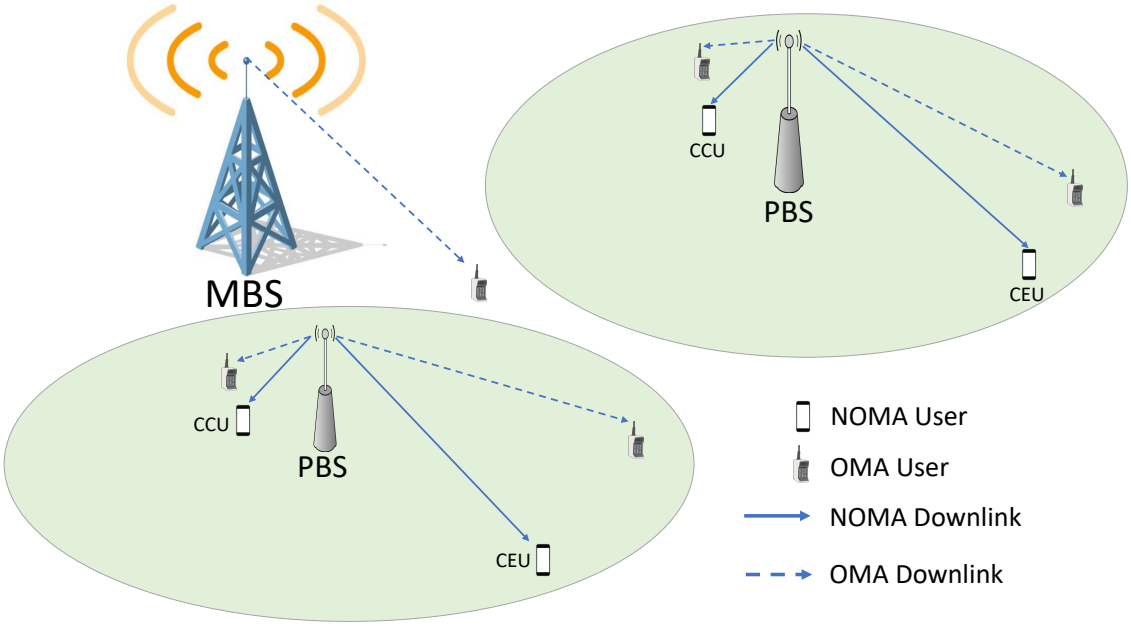

Figure 3.2: System Model of HCN NOMA

study of system performance across different noise environments, an aspect that, to the authors' knowledge, has not been thoroughly explored in the existing literature. This letter presents several noteworthy contributions, detailed as follows: (1) To ensure mathematical tractability and spatial consistency, we utilized PPP within the HCN to model the spatial distributions of both MBS and PBS; (2) This study compares HCN-NOMA and OMA systems under Im-N, deriving closed-form OP expressions for both AWGN and Im-N scenarios; (3) Exploring the interplay between impulse noise occurrence probability and impulsive-to-Gaussian noise power ratio reveals their combined impact on system performance; and (4) Simulation results illustrate the superior spectral and energy efficiencies of the HCN-NOMA system compared to the OMA system both in the AWGN and Im-N scenarios.

3.2 System Model

A two-tier HCN, integrated NOMA with MBS and NOMA-enabled PBS enhances system flexibility, accommodating users with distinct channel conditions and diverse QoS requirements in the shared downlink spectrum is shown in Fig. 3.2. PPP is utilized in HCN for the mathematical modeling of MBS and PBS distributions, offering a spatially realistic framework for wireless network performance evaluation and system design. Nodes and BSs are independently distributed using PPP (Ω_t, λ_t)

for tiers ($t \in \{m, p\}$), and users are distributed via PPP Ω_u with density λ_u [27]. Without loss of generality, each UE, or BS, is equipped with a single antenna and operates in half-duplex mode.

The connectivity between a MBS and a MU adheres to the nearest neighbor connection policy. A bounded path loss model denoted by $P(r) = \frac{1}{1+r_t^{\nu_t}}$ [27] is considered. The path loss exponent for the t-th tier is denoted by ν_t, with r_t representing the distance between the serving BS and the typical user. Consequently, $|h_t|^2 = |\tilde{h}_t|^2 P(r)$ defines the total channel gain experienced by the selected user in the t-th tier, where $\tilde{h}_t \sim \mathcal{CN}(0, 1)$. The system-wide transmission bandwidth is set at 1 Hz, and R denotes the desired data rate for the specific user. The $\tilde{h}_t$ represents the actual complex Gaussian distributed channel, where $|h|^2$ and $|\ddot{h}|^2$ denotes ordered and unordered channel gains, respectively.

3.3 Mathematical analysis

3.3.1 PBS User's SINR (without NOMA)

Mathematical expression of the signal transmitted from the PBS is denoted as $X_{p,tx} = x_p\sqrt{P_p}$, where x_p represents the intended signal to the specific user linked to PBS (PU), and P_p denotes the transmit power of the PBS tier. While the signal received at the PU is represented as

$$X_{p,rx} = \sqrt{P_p}\ddot{h}_{p_o}x_p + \underbrace{\sum_{t\in(m,p)}\sqrt{P_t}x_t\sum_{r\in\Omega_t\setminus\{p_o\}}\ddot{h}_r}_{\text{Intra-tier and Inter-tier interference by BSs}} + n_p, \tag{3.1}$$

where the total noise n_p, modeled by the Bernoulli-Gaussian process, frequently employed in the performance analysis and design of communication systems for its simplicity and effectiveness in characterizing random occurrence of high-power impulses [29], is expressed as

$$n_p = n_w + \delta \times n_I \tag{3.2}$$

where n_w represents the background noise, and n_I represents the Im-N such that $n_w \sim \mathcal{CN}(0, \sigma_w^2)$, and $n_I \sim \mathcal{CN}(0, \sigma_I^2)$. The parameter "$\delta$" follows a Bernoulli process, characterized by an independent and identically distributed (i.i.d.) $0s$ and

1s sequence. It takes the value "1" with probability "p" and "0" with probability "$1-p$". The PDF for the overall noise n_p is detailed in [29], [31], is expressed as,

$$f(n_p) = \frac{(1-p)}{\pi\sigma_w^2} e^{-\frac{|n_p|^2}{\sigma_w^2}} + \frac{p}{\pi(\sigma_w^2+\sigma_I^2)} e^{-\frac{|n_p|^2}{\sigma_w^2+\sigma_I^2}} \tag{3.3}$$

The average noise power ζ is given by [32]

$$\begin{aligned} \zeta &= \mathbb{E}[n_p^2] = \mathbb{E}[n_w^2] + \mathbb{E}[\delta^2] \times \mathbb{E}[n_I^2] \\ &= \sigma_w^2 + p \times \sigma_I^2 = \sigma_w^2 \times \zeta_p \end{aligned} \tag{3.4}$$

where ζ_p is given as $1 + p\lambda$ such that $\lambda = \frac{\sigma_I^2}{\sigma_w^2}$ quantifies the impulsive-to-Gaussian noise power ratio. The SINR at a selected PU can be expressed as [27]

$$\gamma_p = \frac{P_p |\ddot{h}^{p_o}|^2}{\sum_t P_t^{\imath} \mathbb{I}_t + \sigma_w^2 + p\sigma_I^2} = \frac{\rho_p P_p |\ddot{h}^{p_o}|^2}{\sum_t \rho_t^{\imath} \mathbb{I}_t + \zeta_p} \tag{3.5}$$

where ρ_p is the transmit SNR at the PBS tier and is determined as $\rho_p = \mathbb{E}\left[x_p^2\right]/\sigma_w^2$. The transmit SNR from the t-th tier, which interferes with the selected PU is given as $\rho_t^{\imath} = P_t/\sigma_w^2$. Without loss of generality, if the selected PU is situated at the point of origin and the designated PBS is positioned at p_o, according to Slivnyak's theorem [33], $\rho_p^{\imath}\mathbb{I}_p$ denotes the intra-tier interference caused by the PBS tier on the PU. In this case, $\mathbb{I}_p = \sum_{j\in\Omega_p\setminus\{p_o\}} |\ddot{h}_j|^2$, where $|\ddot{h}_j|^2$ is the overall channel gain from the j-th PBS to the selected PU. Likewise, $\rho_m^{\imath}\mathbb{I}_m$ denotes inter-tier interference originating from the MBS tier towards the selected PU. In such case, $\mathbb{I}_m = \sum_{i\in\Omega_m} |\ddot{h}_i|^2$, where $|\ddot{h}_i|^2$ represents the total channel gain for the selected PU from the i-th transmitter of the MBS tier.

3.3.2 PBS User's SINR (with NOMA)

The power domain NOMA is applied by the PBS to support M_p users, where the power allocation factors $a_1 \geq \cdots \geq a_{M_p}$ are determined according to the sorted channel gains $|h_1^{p_o}|^2 \leq \cdots \leq |h_{M_p}^{p_o}|^2$ of the NOMA users. In NOMA, a_n signifies the power coefficients for the n-th user. In this context, a 'near user' or 'CCU' is defined by having a strong channel gain, whereas a 'far user' or 'CEU' has a weaker channel gain. Assuming uniform signal power for all NOMA users, the i-th NOMA user's intended signal is expressed as x_i, while the transmitted signal by the PBS is

Table 3.1: Comparative Analysis with Related Studies

	[24]	[26]	[27]	[31]	[34]	[35]	This work
	HCN+NOMA			NOMA+Im-N			
HCN multi-tier analysis	✓	✓	✓				✓
NOMA	✓	✓	✓	✓	✓	✓	✓
PPP distributions	✓	✓	✓				✓
OP/BER	✓	✓	✓	✓	✓	✓	✓
System Throughput			✓				✓
Energy Efficiency			✓				✓
Im-N environment				✓	✓	✓	✓
Compare: OMA/NOMA	✓	✓	✓		✓		✓
Compare: AWGN/Im-N				✓		✓	✓

represented by $X_{p,tx} = \sum_{i=1}^{M_p} x_i \sqrt{a_i P_p}$. Without loss of generality, we assume that $\mathbb{E}\left[|x_i|^2 = 1\right]$. The signal received by the k-th user is expressed as

$$X_{k,rx}^{p} = h_k^{p_o} s_k \sqrt{P_p} + \underbrace{\sum_{t\in(m,p)} x_t \sqrt{P_t} \sum_{r\in\Omega_t\setminus\{p_o\}} h_r}_{\text{Intra-tier and Inter-tier interference by BSs}} + n_k, \tag{3.6}$$

where s_k comprises of $s_k = \sqrt{a_k} x_k + \sum_{u=k+1}^{M_p} \sqrt{a_u} x_u$. The k-th user performs SIC by decoding the message of the j-th user; thus, the SINR at the k-th user, where $j \leq k$, is denoted as

$$\gamma_{j\to k}^{p} = \frac{\rho_p P_p a_j |h_k^{p_o}|^2}{\rho_p P_p |h_k^{p_o}|^2 \left(\sum_{n=j+1}^{M_p} a_n\right) + \sum_t \rho_t^i \mathbb{I}_t + \zeta_p} \tag{3.7}$$

and a_n is the power allocation factor for users indexed by $n \in \{k, j\}$. The user at the maximum distance from the BS remains uninfluenced by i-SIC, since no SIC is performed, treating signals from other users as noise. Expressing the SINR for the k-th user decoding its own message as

$$\gamma_{k}^{p} = \frac{\rho_p P_p a_k |h_k^{p_o}|^2}{\rho_p P_p |h_k^{p_o}|^2 \left(\sum_{n=k+1}^{M_p} a_n\right) + \sum_t \rho_t^i \mathbb{I}_t + \zeta_p}. \tag{3.8}$$

3.4 Outage analysis

In this section, the rate OP is assessed across various tiers for the designated systems. Outage Probability quantifies the likelihood of performance degradation in a wireless link, such as signal loss, lower data rates, or increased errors.

3.4.1 OMA

The rate OP at a typical PU is determined by considering a uniform distance from the PBS, is given by

$$\begin{aligned}\mathbb{P}_O^p &= \Pr\left[W_p \times \log_2(1+\gamma_p) < R\right], \\ &= \Pr\left[|\ddot{h}_{p_o}|^2 < \frac{\phi_p}{\rho_p P_p}\left(\sum_t \rho_t^i \mathbb{I}_t + \zeta_p\right)\right], \end{aligned} \tag{3.9}$$

where, W_p represents the bandwidth assigned to OMA-based PU, and γ_p denotes the SINR at PU, as defined in (3.5), and R indicates the user's desired data rate. Consequently, the SINR threshold is defined as $\phi_p = 2^{2R} - 1$. Thus, the OP can be expressed as,

$$\mathbb{P}_O^p \approx \sum_{q=0}^{Q} b_q^p e^{-\frac{c_q^p \phi_p \zeta_p}{\rho_p P_p}} \prod_t \mathcal{L}_{\mathbb{I}_t}(\rho_t^i s_p). \tag{3.10}$$

where Q strikes a balance between accuracy and complexity, $b_q^p = -w_Q\sqrt{1-\theta_q^2}\left(\frac{1}{2}\left(\theta_q+1\right)\right)$, $w_Q = \frac{\pi}{Q}$, $\theta_q = \cos\left(\frac{2q-1}{2Q}\pi\right)$, $b_0 = -\sum_{q=1}^{Q} b_q^p$, $c_q^p = 1 + \left(\frac{\mathcal{Y}_p}{2}\theta_q + \frac{\mathcal{Y}_p}{2}\right)_p^{\nu}$, $c_0 = 0$, and $s_p = \frac{c_q^p \phi_p}{\rho_p P_p}$, such that $\mathcal{Y}_p$ denotes coverage range of PBS tier.

Laplace transform of interference from the t-th tier is $\mathcal{L}_{\mathbb{I}_t}(s)$ expressed [27] as

$$\mathcal{L}_{\mathbb{I}_t}(s) = e^{\pi\lambda_t(s^{\mu_t}\Gamma(1-\mu_t,s) - s^{\mu_t}\Gamma(1-\mu_t))}, \tag{3.11}$$

where $\mu_t = 2/\nu_t$, $\Gamma(z) = \int_0^\infty x^{z-1}e^{-x}dx$ and $\Gamma(z,x) = \int_x^\infty t^{z-1}e^{-t}dt$.

Proof

Assuming a homogeneous PPP and utilizing polar coordinates, the CDF of the unordered channel gain in the PBS tier is formulated as [24]:

$$F_{|\ddot{h}_{p_o}|^2}(y) = \frac{2}{\mathcal{Y}_p^2}\int_0^{\mathcal{Y}_p}(1-e^{-\left(1+r_p^{\nu_p}\right)y})r_p dr_p. \tag{3.12}$$

Using the GC quadrature method [**?**] on equation (3.12), we obtain

$$F_{|\ddot{h}_{p_o}|^2}(y) \simeq \sum_{q=0}^{Q} b_q^p e^{-c_q^p y}, \tag{3.13}$$

Thus, the OP, as expressed in (3.9), can be reformulated as,

$$\mathbb{P}_O^p \approx \sum_{q=0}^{Q} b_q^p e^{-c_q^p\left\{\frac{\phi_p}{\rho_p P_p}\left(\sum_t \rho_t^i \mathbb{I}_t+\zeta_p\right)\right\}}. \tag{3.14}$$

By solving (3.14), the result leads directly to the expression given in (3.10).

3.4.2 Outage Analysis for PBS Tier (NOMA)

We examine a scenario where the user's QoS requirements specify a predefined target data rate R, leading to the formulation of the OP as follows:

$$\mathbb{P}_k^{O,p} = \Pr\left[\gamma_k^p < \phi_k, \gamma_{j\to k}^p < \phi_j\right], \tag{3.15}$$

where $\gamma_{j\to k}^p$ and γ_k^p are given in (3.7), and (3.8) respectively.
Given the uniform distance from the PBS and considering the ordered channel gains, the rate OP at the k-th selected PU is given by

$$\begin{aligned}\mathbb{P}_k^{O,p} \approx & \epsilon_k \sum_{d=0}^{M_p-k}\binom{M_p-k}{d}\frac{(-1)^d}{k+d}\sum_{T_k^d}\binom{k+d}{l_0+...+l_N}\prod_{q=0}^{Q}(b_q^p)^{l_q} \\ & \times e^{-\sum_{q=0}^{Q} l_q \frac{c_q^p \psi_{\max}\zeta_p}{\rho_p P_p}}\prod_t \mathcal{L}_{\mathbb{I}_t}(\rho_t^i s_p),\end{aligned} \tag{3.16}$$

where $\epsilon_k = \frac{M_p!}{(k-1)!(M_p-k)!}$, $s_p = \frac{\psi_{\max}\sum_{q=0}^{Q} l_q c_q^p}{\rho_p P_p}$, $T_k^d = \left\{(l_0,...,l_N)|\sum_{i=0}^{N} l_i = k+d\right\}$, and $\binom{k+d}{l_0+...+l_N} = \frac{(k+d)!}{l_0!...l_N!}$.

Proof

As the successful self-message decoding in SIC directly impacts the OP, it can be expressed for the k-th user as:

$$\mathbb{P}_k^{O,p} = \Pr\left[|h_k^{p_o}|^2 < \frac{\psi_{max}\left(\sum_t \rho_t^i \mathbb{I}_t + \zeta_p\right)}{\rho_p P_p}\right]. \tag{3.17}$$

This results in the OP as $\mathbb{P}_k^{O,p} = F_{|h_k^{p_o}|^2}(y)$, where $y = \frac{\psi_{max}\left(\sum_t \rho_t^i \mathbb{I}_t + \zeta_p\right)}{\rho_p P_p}$ and $\psi_{max} = \max(\psi_1, \psi_2, \ldots, \psi_k)$. For a CEU when $k = 1$, OP is simply calculated with $y = \frac{\psi_j\left(\sum_t \rho_t^i \mathbb{I}_t + \zeta_p\right)}{\rho_p P_p}$, as it decodes its own message without performing SIC. $\psi_j = \frac{\phi_j}{a_j - \phi_j\left(\sum_{l=j+1}^{M_p} a_l\right)}$, where, ϕ_j is defined as $2^{R_j} - 1$, with R_j representing the target data rate for the j-th user.

The connection between the CDF of ordered and unordered channel gains of the PBS tier is expressed as follows [**?**]:

$$F_{|h_k^{p_o}|^2}(y) = \epsilon_k \sum_{d=0}^{M_p-k} \binom{M_p - k}{d} \frac{(-1)^d}{k+d} \left(F_{|\ddot{h}_{p_o}|^2}(y)\right)^{k+d}. \tag{3.18}$$

Upon substituting (3.13) in (3.18) and employing the multinomial theorem, the CDF for the ordered channel gains is obtained as

$$\begin{aligned} F_{|h_k^{p_o}|^2}(y) \simeq & \epsilon_k \sum_{d=0}^{M_p-k} \binom{M_p - k}{d} \frac{(-1)^d}{k+d} \sum_{T_k^d} \binom{k+d}{l_0 + \ldots + l_N} \\ & \times \left(\prod_{q=0}^{Q} (b_q^p)^{l_q}\right) e^{-\sum_{q=0}^{Q} l_q c_q^p y}. \end{aligned} \tag{3.19}$$

Upon substituting "y" into (3.19) and solving it yields the expression presented in (3.16).

3.5 System Throughput analysis

In this section, we investigate the throughput performance of a NOMA-based HCN operating under an impulsive noise environment, specifically considering two-user scenarios. Throughput serves as a fundamental indicator of system efficiency, reflecting the average data rate successfully delivered to users per unit bandwidth while accounting for the effects of channel imperfections, noise disturbances, and

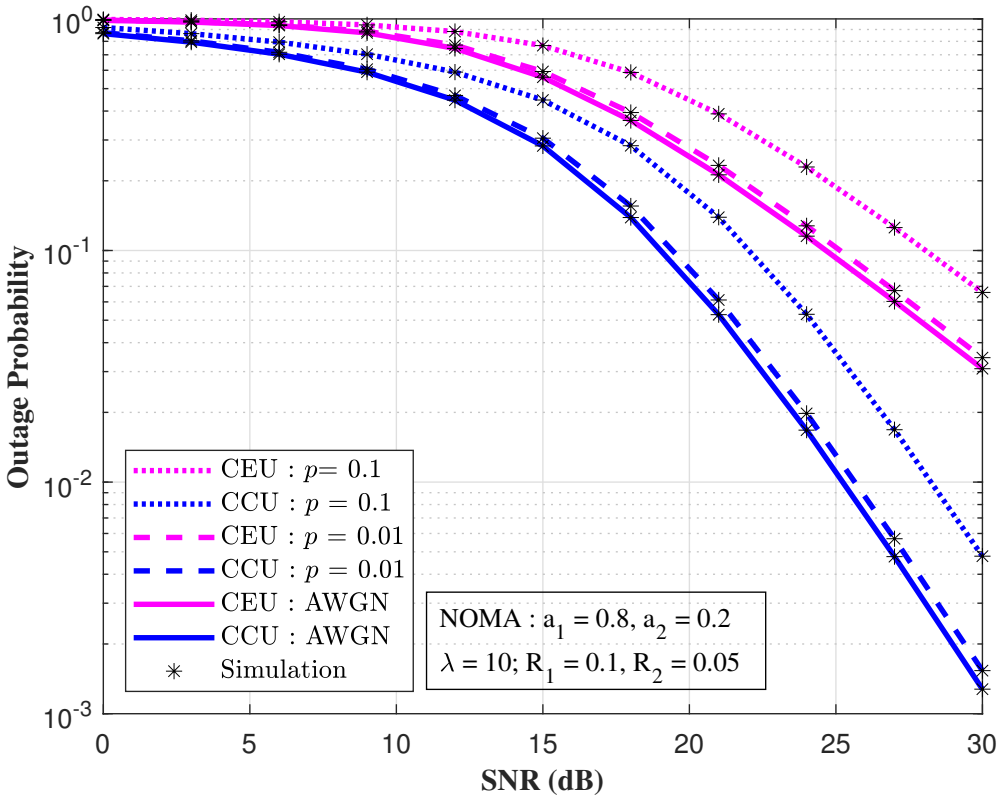

Figure 3.3: OP across multiple occurrence probability of Im-N utilizing NOMA.

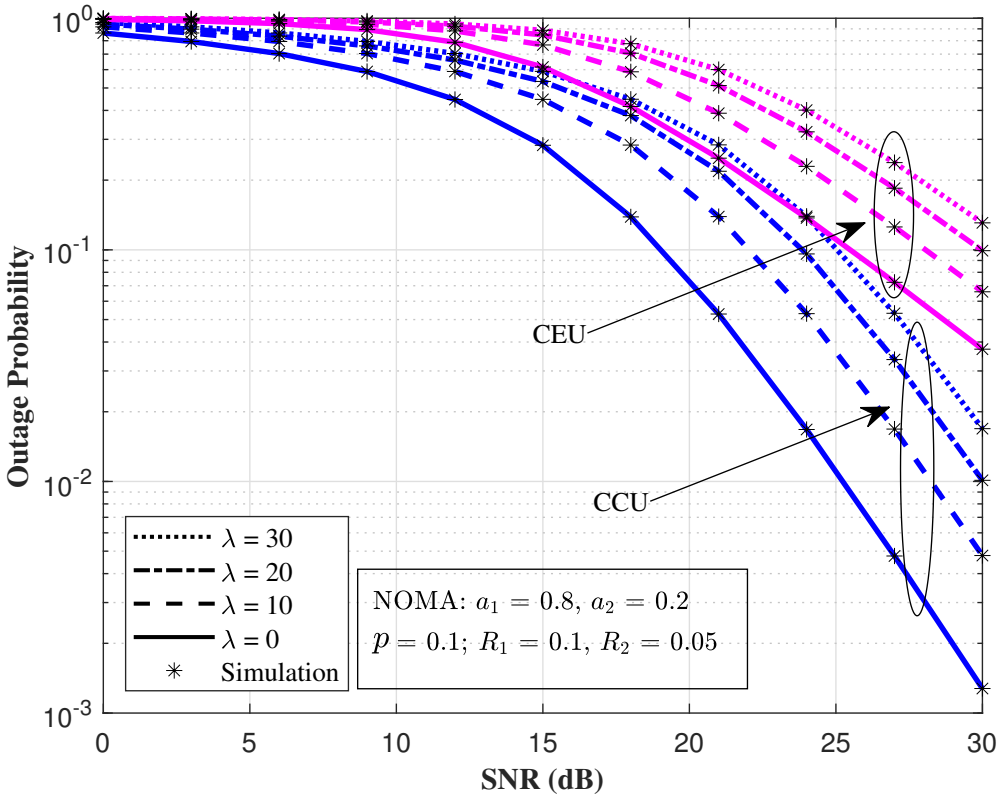

Figure 3.4: OP across different impulsive to Gaussian noise power ratio utilizing NOMA.

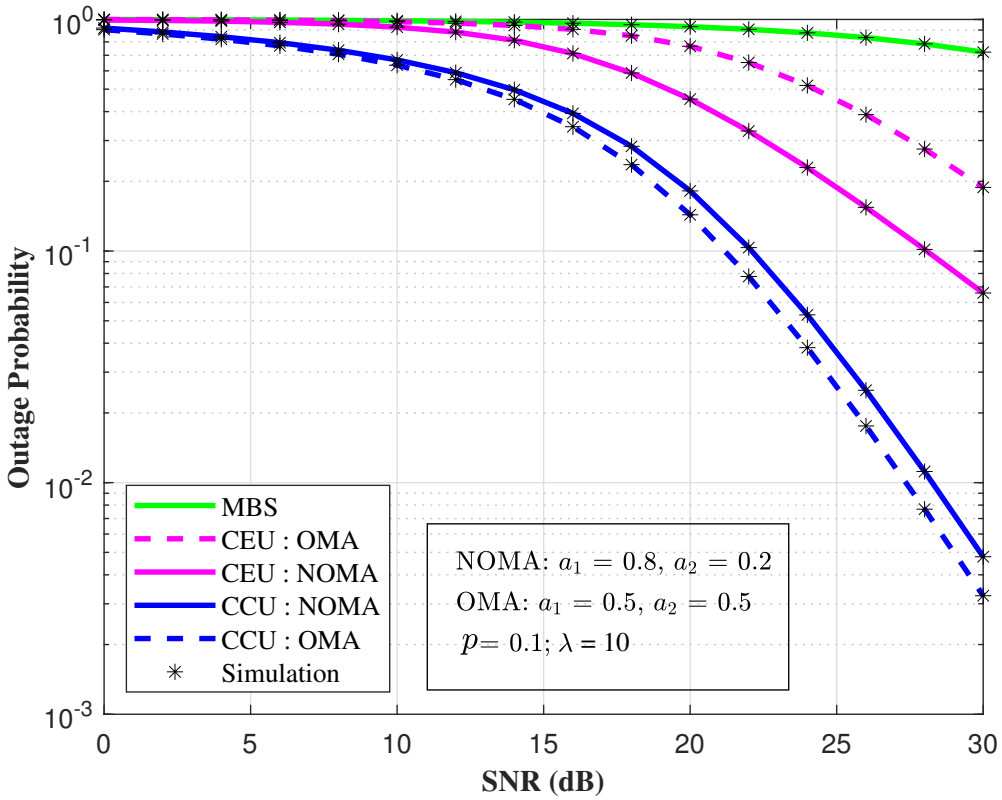

Figure 3.5: OP for both OMA and NOMA subject to impulsive noise.

outage events.

The system throughput, denoted as τ_{sys} (in bps/Hz), is mathematically defined as

$$\tau_{\text{sys}} = \left(1 - P_{\text{O},p}^{\text{CEU}}\right) R_1 + \left(1 - P_{\text{O},p}^{\text{CCU}}\right) R_2, \tag{3.20}$$

where $P_{\text{O},p}^{\text{CEU}}$ and $P_{\text{O},p}^{\text{CCU}}$ represent the OP experienced by the CEU and the CCU, respectively. R_1 and R_2 denote the target data rates assigned to the CEU and CCU.

This expression clearly illustrates that the system throughput is influenced not only by the intended data rates but also by the reliability of the links, which are significantly affected by the harsh Im-N characteristics prevalent in the environment. The analysis particularly emphasizes how Im-N degrades the robustness of user transmissions in NOMA systems, making reliable link adaptation and outage control critical for optimal network performance.

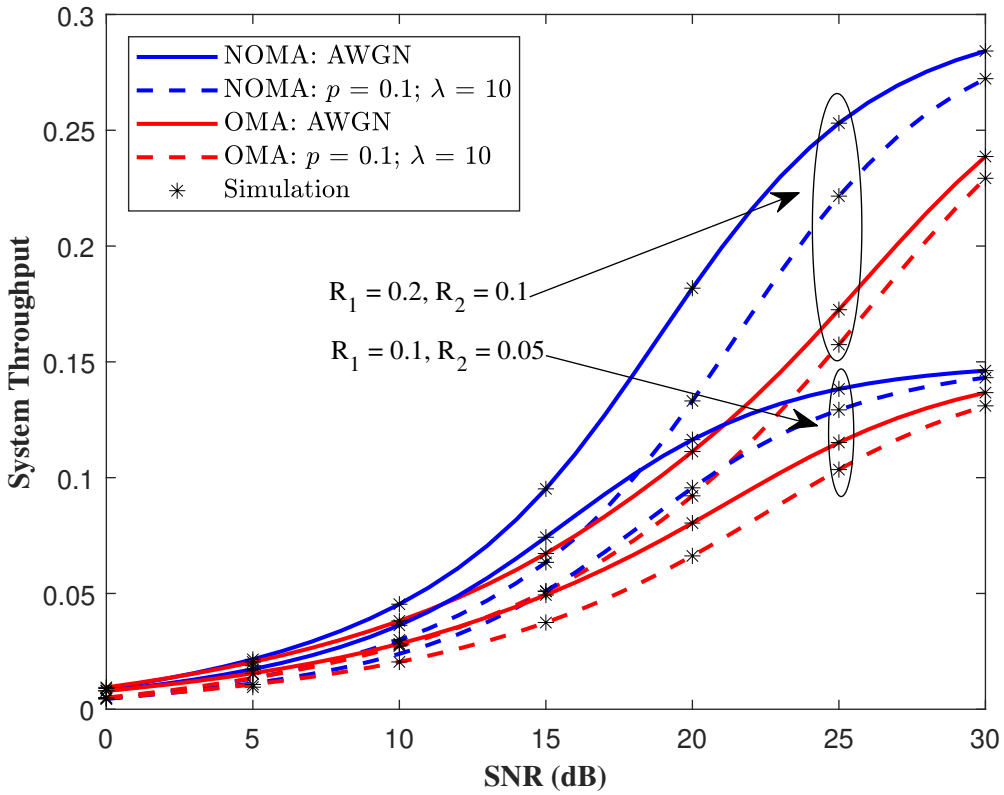

Figure 3.6: SE in HCN using OMA and NOMA subject to Im-N.

3.6 Energy Efficiency analysis

In this section, we evaluate the EE performance of the considered NOMA-based HCN operating in an Im-N environment, particularly focusing on a two-user scenario. Energy efficiency is a critical performance metric that measures the amount of successfully transmitted data per unit of consumed power, thus balancing throughput and power consumption in the system.

The system energy efficiency, denoted by η_{sys} (in bps/Hz/Watt), is defined as

$$\eta_{\text{sys}} = \frac{\tau_{\text{sys}}}{P_p}, \tag{3.21}$$

where τ_{sys} represents the system throughput as defined earlier, and P_p denotes the total transmission power.

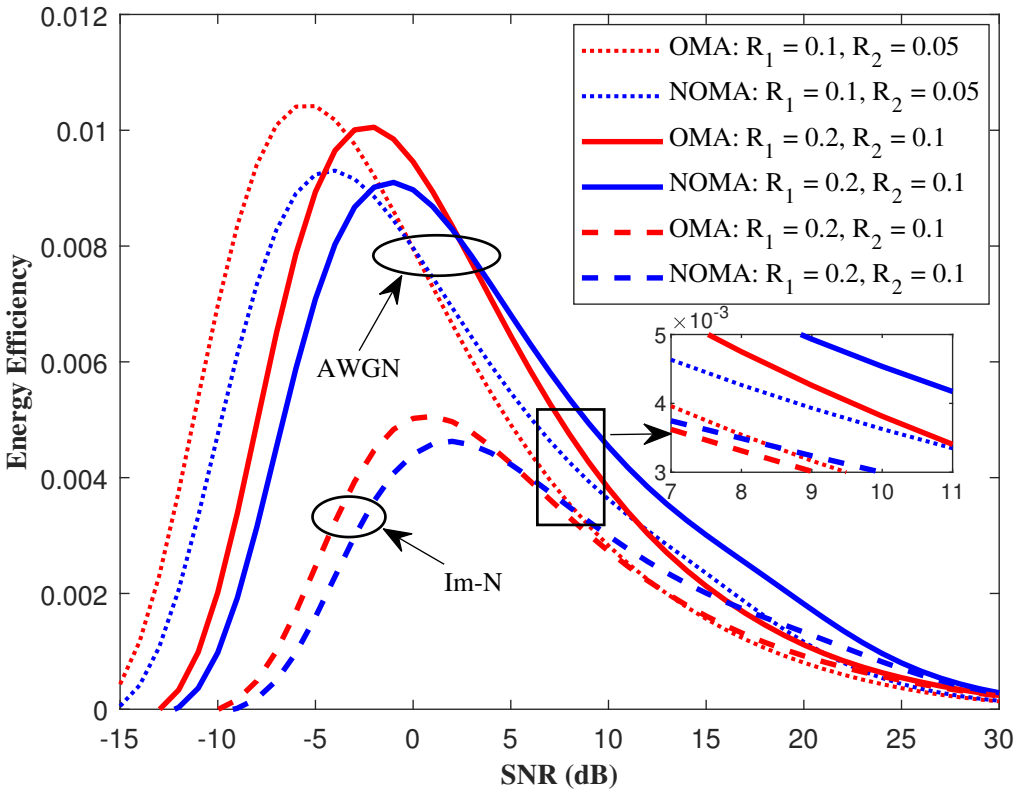

Figure 3.7: Energy Efficiency in HCN using OMA and NOMA subject to Im-N.

3.7 Bar Plot analysis

In this section, we further analyze the performance gains achieved by NOMA over traditional OMA schemes in an Im-N environment by examining the SE improvement across various SNR levels. The SE gain highlights the percentage improvement in data transmission efficiency when NOMA is employed compared to OMA, making it a valuable metric for performance comparison.

The SE gain, denoted by G_{SE} (in %), can be calculated as

$$G_{\text{SE}} = \frac{\tau_{\text{NOMA}} - \tau_{\text{OMA}}}{\tau_{\text{OMA}}} \times 100, \tag{3.22}$$

where τ_{NOMA} and τ_{OMA} denote the system throughput values for the NOMA and OMA schemes, respectively.

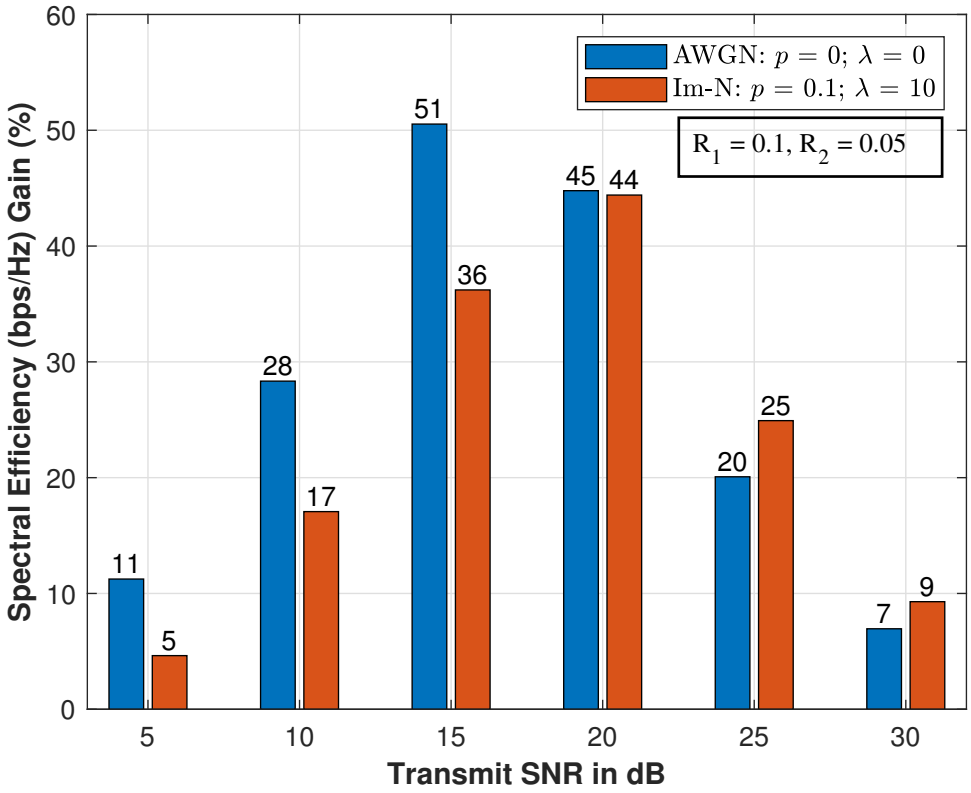

Figure 3.8: Quantitative analysis: Comparing NOMA vs. OMA gain (%) subject to Im-N.

3.8 Discussions on numerical and simulation results

In this section, inferences are drawn based on the simulation results on the OP, from which system throughput and EE are derived. The analytical results are validated using simulations, with parameters including MBS transmitting power (P_m) set at 40 W and PBS transmitting power (P_p) at 1 W, with MBS node density (λ_m) at $5 \times 10^{-5}\text{m}^{-2}$, PBS node density ($\lambda_p$) at 10^{-4}m^{-2}, and user node density (λ_u) at $5 \times 10^{-4}\text{m}^{-2}$. Power allocation coefficients for NOMA users (a_k) are 0.8 and 0.2. Coverage ranges are set to 1000 m for MBS ($\mathcal{Y}_m$) and 5 m for PBS ($\mathcal{Y}_p$), with path loss exponents of 3 for MBS (ν_m) and 4 for PBS (ν_p). Target data rates for CEU (R_1) and CCU (R_2) are specified as in the respective figures, similar to the ones used by [25], [27], and [31].

3.8.1 Simulation Parameters

Table 3.2: Simulation Parameters

Parameters	**Symbols**	**Value**
Transmitting power from MBS, and PBS	P_m, P_p	40 W, 1 W
MBS, PBS, and user's density	λ_m, λ_p, λ_u	$5 \times 10^{-5}m^{-2}$, $10^{-4}m^{-2}$, $5 \times 10^{-4}m^{-2}$
Coverage range of MBS, PBS	$\mathcal{Y}_m, \mathcal{Y}_p$	1000 m, 5 m
Path loss exponent for MBS, PBS	ν_m, ν_p	$3, 4$
Target data rate	R_1, R_2	$0.1, 0.05$
Occurrence Probability of Impulse noise [31]	p	0.1
Power allocation factor	a_1, a_2	$0.8, 0.2$
Impulsive-to-Gaussian noise power ratio [31]	Λ	10

3.8.2 Numerical Results

The impact of Im-N on the outage performance of the HCN-NOMA system within the PBS tier, considering two users, is illustrated in Fig. 3.3. This figure presents the OP as a function of varying Im-N occurrence probabilities for NOMA-enabled PBS users and compared with AWGN noise. The analysis indicates a substantial degradation in outage performance for both CEU and CCU under impulsive noise, compared to AWGN noise. Notably, for CCUs, the performance improves by approximately 2.617 dB and 0.393 dB as the impulse noise probability is reduced from 0.1 to 0.01 and further to 0, achieving an OP of 10^{-2}. A similar trend is observed for CEUs, where outage performance improves as the occurrence probability of Im-N decreases. This highlights the importance of accounting for and mitigating Im-N in NOMA implementations.

The OP as a function of varying impulsive-to-Gaussian noise power ratios, with a fixed occurrence probability of Im-N, is depicted in Fig. 3.4 for NOMA-enabled PBS users and compared with AWGN noise. The analysis shows that while outage performance improves with increasing SNR, both CEU and CCU experience significant

performance degradation as the impulsive-to-Gaussian noise power ratio increases, underscoring the negative impact of Im-N. Additionally, at $\lambda = 30$, a loss of more than 6 dB for CCU and approximately 5 dB for CEU is observed, achieving an OP of 10^{-1}. This is attributed to the fact that CCUs, benefiting from better channel conditions, are allocated lower transmit power, making them more susceptible to interference and additional Im-N. In contrast, CEUs with higher power allocation are better equipped to withstand such noise, resulting in relatively less degradation in their outage performance.

Fig. 3.5 provides an in-depth comparative analysis of NOMA and OMA performance within an HCN under Im-N. The figure demonstrates that users served by the PBS tier, classified as CEU and CCU, show better performance than those served by the MU. CCUs consistently outperform CEUs across different access schemes within the PBS tier. NOMA provides a performance edge for CEUs, while OMA performs better for CCUs, particularly when specific power allocation coefficients are applied. This is especially evident under varying impulsive noise power ratios and occurrence parameters, underscoring the importance of signal power distribution in these scenarios.

System throughput (bps/Hz) is calculated as $\tau_{sys} = \left(1 - \mathbb{P}_{CEU}^{O,p}\right) R_1 + \left(1 - \mathbb{P}_{CCU}^{O,p}\right) R_2$, where the OP at the PBS tier for the CEU, and CCU, denoted as $\mathbb{P}_{CEU}^{O,p}$ and $\mathbb{P}_{CCU}^{O,p}$ respectively, are determined by operating (3.16) at $k = 1$ and $k = 2$, with R_1 and R_2 denoting the target data rate for the CEU and CCU, as per [25], and [27]. Fig. 3.6 compares the SE of NOMA and OMA systems under Im-N and AWGN scenarios across different target data rates. NOMA shows better overall system performance and higher throughput than OMA in both cases. Increasing signal power improves outage performance for CCUs with minimal negative impact on CEUs. However, both NOMA and OMA experience performance degradation under Im-N conditions compared to AWGN. Despite the overall performance degradation in Im-N, NOMA still achieves higher spectral efficiency than OMA under AWGN conditions, particularly for SNR values above 15 dB, for the given simulation parameters.

Energy efficiency, defined as the ratio of system throughput to total energy consumed ($\eta_{sys} = \tau_{sys} \div P_p$), is analyzed for both NOMA and OMA systems in Fig. 3.7 under Im-N and AWGN scenarios across different target data rates, where τ_{sys} is system throughput, and P_p is transmit power at the PBS [**?**]. In the HCN-NOMA

system, energy efficiency initially increases with rising SNR, reaching a peak at specific SNR values before declining as SNR continues to increase. This decline occurs because, in the high SNR regime, the network consumes more power relative to the achieved system throughput. The analysis shows that energy efficiency peaks at $\approx 9.1 \times 10^{-3}$ at -1.0 dB for NOMA and $\approx 10.1 \times 10^{-3}$ at -2.0 dB for OMA under the AWGN scenario. Similar trends are observed under the Im-N scenario, though the efficiency values are significantly lower ($\approx 4.63 \times 10^{-3}$ at 2.0 dB for NOMA and $\approx 5.06 \times 10^{-3}$ at 1.0 dB for OMA) compared to AWGN. These peaks are noted when the system targets fixed data rates of 0.2 and 0.1 for CEUs and CCUs, respectively. NOMA consistently outperforms OMA across the positive SNR spectrum, especially at higher SNRs, with a slight shift towards higher peak energy efficiency at lower SNRs for lower target data rates. NOMA outperforms OMA at higher SNRs in the Im-N scenario ($\approx$ 5.5 dB) compared to AWGN ($\approx$ 2.35 dB) due to the dominant noise in Im-N environment requiring higher SNR for better NOMA performance.

In Fig. 3.8, the analysis shows that NOMA significantly outperforms OMA in terms of SE, with gains of 51%, 45%, 20%, and 7% at transmit SNR levels of 15, 20, 25, and 30 dB under AWGN. However, these gain margins fluctuate with varying SNRs, reflecting the non-linear impact of OP on system throughput. Under AWGN, NOMA shows better performance compared to OMA at lower transmit SNRs due to reduced noise impact, while in the Im-N environment as noise becomes the dominant factor, NOMA outperforms at higher transmit SNRs, underscoring the need for operating in higher SNRs under such scenarios.

3.9 Summary

This Chapter compares the impact of Im-N in an HCN downlink NOMA system. The findings highlight substantial impact on the outage performance, system throughput, and energy efficiency within the HCN-NOMA system, particularly under different data rate scenarios. Numerical findings show NOMA's superiority over OMA, particularly under AWGN as well as Im-N scenario, across a broad SNR range. The results highlight NOMA's superior performance in AWGN scenarios, especially at lower SNRs; however, its effectiveness decreases in Im-N conditions, underscoring the need for operating in higher SNRs. This analysis emphasizes the need for careful decision-making in deploying NOMA techniques in HCN under dif-

ferent noise conditions. CSI precision is critical for NOMA's SIC, and future work should examine the impact of imperfect CSI on PPP-distributed users in NOMA systems, considering both perfect and i-SIC within an HCN, using this study as a benchmark.

While the preceding analysis confirms NOMA's robustness even under Im-N, it raises further questions about the broader implications and comparative trade-offs with respect to SE, outage behavior, and energy performance. The concluding chapter distills these findings, offers key insights, and outlines potential directions for future research in enhancing the resilience and applicability of NOMA-based systems.

CHAPTER 4

CONCLUSIONS AND FUTURE WORKS

This chapter presents the findings drawn from the work done in this thesis, as well as potential avenues for future work.

4.1 Conclusions

Building upon the layered exploration of system impairments and noise environments in previous chapters, this concluding section synthesizes the major outcomes and discusses their relevance for future 6G network design and deployment strategies. In this thesis, we presented a comprehensive performance analysis of HCNs employing NOMA under realistic communication impairments. Two major aspects were studied in depth: the impact of Im-N and the effects of HI and i-CSI on NOMA-enabled HCNs.

First, the study addressed the realistic constraints of hardware imperfections and channel estimation errors. Analytical models were developed to capture the combined effect of HI and i-CSI on the system performance. Despite the degradation introduced by practical impairments, results confirmed that NOMA retains substantial performance gains over OMA, especially in terms of outage probability and system throughput. The findings validate that NOMA remains a viable access scheme for next-generation wireless networks even under non-ideal hardware and imperfect CSI conditions.

Secondly, the performance of HCN-NOMA systems operating under impulsive noise environments was investigated. Using stochastic geometry-based modeling, analytical expressions for key performance metrics such as outage probability, system throughput, and EE were derived. Comparative results demonstrated that NOMA consistently outperforms traditional OMA, achieving superior SE and EE across a

broad range of SNRs. Although Im-N degrades overall system performance compared to AWGN conditions, NOMA maintains a distinct advantage, particularly at higher SNRs, making it a strong candidate for deployment in industrial and urban scenarios characterized by impulsive electromagnetic interference.

Overall, the thesis demonstrates that while practical impairments such as Im-N, hardware distortions, and channel estimation errors can significantly impact system performance, NOMA consistently outperforms OMA under various adverse conditions. These results reinforce the potential of NOMA to meet the stringent requirements of future 6G networks in terms of high spectral efficiency, massive connectivity, and EE. Future work may extend this study by exploring robust power control, advanced SIC techniques, and machine learning-based solutions for adaptive resource allocation in realistic HCN-NOMA deployments.

4.2 Future Works

Building on the findings of this study, several promising directions for future research are outlined:

- **Integration of HIs and Im-N:** A natural extension would be to jointly analyze the combined effect of HI, i-CSI, and Im-N on the performance of HCN-NOMA systems. This would provide a more realistic evaluation under practical deployment conditions.

- **Advanced SIC Techniques under Im-N:** Future work can focus on developing advanced or adaptive SIC algorithms that are robust to the presence of Im-N and i-CSI, thereby enhancing the reliability of NOMA communications.

- **Energy Harvesting and SWIPT-enabled HCNs:** Integrating energy harvesting and SWIPT mechanisms into HCN-NOMA systems under HI, i-CSI, and Im-N scenarios could enable sustainable network operation, especially in IoT applications.

- **IRS-assisted HCN-NOMA under Practical Impairments:** Intelligent reflecting surfaces (IRS) can be investigated as a tool to enhance the performance of HCN-NOMA systems under hardware impairments, imperfect CSI, and impulsive noise environments.

- **Dynamic Power Allocation Strategies:** The development of dynamic and adaptive power control strategies that consider real-time noise characteristics and HI metrics can further optimize system throughput and reliability.

- **Impact of i-CSI and SIC in Im-N Environments:** Investigating the impact of i-CSI and SIC on NOMA-enabled HCNs operating under Im-N environments would provide deeper insights into practical system performance limits.

- **Modeling with Repulsive Point Processes:** Instead of using the traditional PPP, future research can explore repulsive models such as the RPP to better capture spatial user and base station distributions and to reduce interference in dense deployments.

REFERENCES

[1] M. Al-Imari, P. Xiao, M. A. Imran, and R. Tafazolli,"Uplink non-orthogonal multiple access for 5G wireless networks," IEEE Wireless Communications Letters, vol. 4, no. 5, pp. 529–532, Oct. 2015.

[2] Liu, Yuanwei and Zhang, Shuowen and Mu, Xidong and Ding, Zhiguo and Schober, Robert and Al-Dhahir, Naofal and Hossain, Ekram and Shen, Xuemin, "Evolution of NOMA toward next generation multiple access (NGMA) for 6G," IEEE J. Sel. Areas Commun., vol. 40, no. 4, pp. 1037–1071, 2022.

[3] J. B. Andersen, T. S. Rappaport, and S. Yoshida, "Propagation measurements and models for wireless communications channels," IEEE Communications Magazine, vol. 33, no. 1, pp. 42–49, Jan. 1995.

[4] Z. Ding, F. Adachi, and H. V. Poor, "The application of MIMO to non-orthogonal multiple access," IEEE Transactions on Wireless Communications, vol. 15, no. 1, pp. 537–552, Jan. 2016.

[5] L. Cohen, "Methods for Testing Impulse Noise Tolerance," IEEE 802.3bz Task Force Meeting, May 2015.

[6] Duan, H., Mirzaei,"A. Adaptive Rate Maximization and Hierarchical Resource Management for Underlay Spectrum Sharing NOMA HetNets with Hybrid Power Supplies," Mobile Netw Appl 28, 1145–1161 (2023).

[7] A. S. Parihar, K. Singh, V. Bhatia, C.-P. Li, and T. Q. Duong, "Perfor mance Analysis of NOMA Enabled Active RIS-Aided MIMO Hetero geneous IoT Net-

works With Integrated Sensing and Communication," IEEE Internet Things J., pp. 1–1, 2024.

[8] Z. Ding, X. Lei, G. K. Karagiannidis, R. Schober, J. Yuan, and V. K. Bhargava, "A survey on non-orthogonal multiple access for 5G networks: Research challenges and future trends," IEEE J. Sel. Areas Commun., vol. 35, no. 10, pp. 2181–2195, Oct. 2017.

[9] Y. Liu, S. Zhang, X. Mu, Z. Ding, R. Schober, N. Al-Dhahir, E. Hossain, and X. Shen, "Evolution of NOMA toward next generation multiple access (NGMA) for 6G," IEEE J. Sel. Areas Commun., vol. 40, no. 4, pp. 1037–1071, Apr. 2022.

[10] Z. Ding, R. Schober, and H. V. Poor, "Unveiling the importance of SIC in NOMA systems—Part 1: State of the art and recent findings," IEEE Commun. Lett., vol. 24, no. 11, pp. 2373–2377, Nov. 2020.

[11] C. Zhao, Y. Liu, Y. Cai, M. Zhao, and Z. Ding, "Non-Orthogonal Multiple Access for UAV-Aided Heterogeneous Networks: A Stochastic Geometry Model," IEEE Trans. Veh. Technol., vol. 72, no. 1, pp. 940 956, Jan. 2023.

[12] A. S. Parihar, A. Baghel, P. Swami, and V. Bhatia, "On Performance of SWIPT Empowered NOMA-HetNet with Non-Linear Energy Harvest ing," in Proc. Nat. Conf. Commun. (NCC), 2024, pp. 1–6.

[13] Y. Liu, Z. Ding, M. Elkashlan, and H. V. Poor, "Cooperative Non orthogonal Multiple Access With Simultaneous Wireless Information and Power Transfer," IEEE J. Sel. Areas Commun., vol. 34, no. 4, pp. 938–953, Apr. 2016.

[14] A. S. Parihar, P. Swami, V. Bhatia, and Z. Ding, "Performance analysis of SWIPT enabled cooperative-NOMA in heterogeneous networks using carrier sensing," IEEE Trans. Veh. Technol., vol. 70, no. 10, pp. 10646 10656, Oct. 2021.

[15] S. Bisen, P. Shaik, and V. Bhatia, "On Performance of Energy Harvested Cooperative NOMA Under Imperfect CSI and Imperfect SIC," IEEE Trans. Veh. Technol., vol. 70, no. 9, pp. 8993–9005, Sep. 2021.

[16] A. Baghel, A. S. Parihar, V. Bhatia, K. Choi, and A. K. Mishra, "On Joint Impact of HPA Non-Linearity and Imperfect SIC in NOMA Enabled HCN Using Stochastic Geometry," IEEE Trans. Veh. Technol., vol. 73, no. 6, pp. 8055–8068, Jun. 2024.

[17] M. Katwe, K. Singh, C.-P. Li, and Z. Ding, "Spectral-Efficient Downlink Systems Under Imperfect SIC and CSI: MC-NOMA or Partial NOMA?" IEEE Wireless Commun. Lett., vol. 13, no. 1, pp. 133–137, Jan. 2024.

[18] A. Baghel, A. S. Parihar, K. Choi, and V. Bhatia, "On Impact of HPA Non-linearity in NOMA Enabled Heterogeneous Cellular Network," IEEE Trans. Veh. Technol., pp. 1–6, 2024.

[19] Y. Hmamouche, M. Benjillali, S. Saoudi, H. Yanikomeroglu, and M. Di Renzo, "New trends in stochastic geometry for wireless networks: A tutorial and survey," Proc. IEEE, vol. 109, no. 7, pp. 1200–1252, 2021.

[20] Y. Liu, Z. Ding, M. Elkashlan, and J. Yuan, "Nonorthogonal multiple access in large-scale underlay cognitive radio networks," IEEE Trans. Veh. Technol., vol. 65, no. 12, pp. 10 152–10 157, Dec. 2016.

[21] A. S. Parihar, P. Swami, and V. Bhatia, "On Performance of SWIPT En- abled PPP Distributed Cooperative NOMA Networks Using Stochastic Geometry," IEEE Trans. Veh. Technol., vol. 71, no. 5, pp. 5639–5644, 2022.

[22] Z. Ding, X. Lei, G. K. Karagiannidis, R. Schober, J. Yuan, and V. K. Bhargava, "A survey on non-orthogonal multiple access for 5G networks: Research challenges and future trends," *IEEE J. Sel. Areas Commun.*, vol. 35, no. 10, pp. 2181–2195, Oct. 2017.

[23] Y. Liu, S. Zhang, X. Mu, Z. Ding, R. Schober, N. Al-Dhahir, E. Hossain, and X. Shen, "Evolution of NOMA toward next generation multiple access (NGMA) for 6G," *IEEE J. Sel. Areas Commun.*, vol. 40, no. 4, pp. 1037–1071, Apr. 2022.

[24] P. Swami, V. Bhatia, S. Vuppala, and T. Ratnarajah, "A cooperation scheme for user fairness and performance enhancement in NOMA HCN," *IEEE Trans. Veh. Technol.*, vol. 67, no. 12, pp. 11965–11978, Dec. 2018.

[25] A. S. Parihar, P. Swami, and V. Bhatia, "On performance of SWIPT enabled PPP distributed cooperative NOMA networks using stochastic geometry," *IEEE Trans. Veh. Technol.*, vol. 71, no. 5, pp. 5639–5644, May 2022.

[26] C. Zhao, Y. Liu, Y. Cai, M. Zhao, and Z. Ding, "Non-Orthogonal Multiple Access for UAV-Aided Heterogeneous Networks: A Stochastic Geometry Model," *IEEE Trans. Veh. Technol.*, vol. 72, no. 1, pp. 940–956, Jan. 2023.

[27] A. Baghel, A. S. Parihar, V. Bhatia, K. Choi, and A. K. Mishra, "On Joint Impact of HPA Non-Linearity and Imperfect SIC in NOMA Enabled HCN Using Stochastic Geometry," *IEEE Trans. Veh. Technol.*, vol. 73, no. 6, pp. 8055–8068, Jun. 2024.

[28] M. Cheffena, "Industrial wireless sensor networks: Channel modeling and performance evaluation," *EURASIP J. Wireless Commun. Netw.*, vol. 2012, no. 1, pp. 1–8, Dec. 2012.

[29] T. Bai, H. Zhang, J. Wang, C. Xu, M. Elkashlan, A. Nallanathan, and L. Hanzo, "Fifty years of noise modeling and mitigation in power line communications," *IEEE Commun. Surveys Tuts.*, vol. 23, no. 1, pp. 41–69, 2021.

[30] K. Blackard, T. Rappaport, and C. Bostian, "Measurements and models of radio frequency impulsive noise for indoor wireless communications," *IEEE J. Sel. Areas Commun.*, vol. 11, no. 7, pp. 991–1001, 1993.

[31] B. Selim, M. S. Alam, G. Kaddoum, and B. L. Agba, "Effect of impulsive noise on uplink NOMA systems," *IEEE Trans. Veh. Technol.*, vol. 69, no. 3, pp. 3454–3458, Mar. 2020.

[32] M.Hussain, H.Shakir, and H.Rasheed, "Deep Learning Approaches for Impulse Noise Mitigation and Classification in NOMA-Based Systems," *IEEE Access*, vol.9, pp.143836–143846, Oct.2021.

[33] Y. Hmamouche, M. Benjillali, S. Saoudi, H. Yanikomeroglu, and M. Di Renzo, "New trends in stochastic geometry for wireless networks: A tutorial and survey," *Proc. IEEE*, vol. 109, no. 7, pp. 1200–1252, 2021.

[34] A. Samir, M. Elsayed, A. A. A. El-Banna, K. Wu, and B. M. ElHalawany, "Performance of NOMA-Based Dual-Hop Hybrid Powerline Wireless Commu-

nication Systems," *IEEE Trans. Veh. Technol.*, vol. 71, no. 6, pp. 6548–6558, Jun. 2022.

[35] M. S. Alam, B. Selim, I. Ahmed, G. Kaddoum, and H. Yanikomeroglu, "Bursty Impulsive Noise Mitigation in NOMA: A MAP Receiver-Based Approach," *IEEE Commun. Lett.*, vol. 25, no. 9, pp. 2790–2794, Sep. 2021.

LIST OF PUBLICATIONS

Journals

1. Amit Baghel, Divyanshi Singh, Abhinav Singh Parihar, Peter Brida, Vimal Bhatia, Ondrej Krejcar, Nandana Rajatheva, and Matti Latva-aho, "Performance of Heterogeneous NOMA Networks in Impulsive Noise with Transmit Antenna Selection," *IEEE Wireless Communications Letters*.
2. Amit Baghel, Divyanshi Singh, Abhinav Singh Parihar, Vimal Bhatia, Premanandana Rajatheva and Matti Latva-aho, "Performance Analysis of NOMA in HCN with Hardware Impairments and Imperfect CSI," *IEEE Wireless Communications Letters* (Submitted).

Conferences

1. Amit Baghel, Divyanshi Singh, Vimal Bhatia, Nandana Rajatheva, and Matti Latva-aho, "On Impact of Impulsive Noise on Distributed Heterogeneous Cellular Networks in Industrial IoT," *Proceedings of the IEEE International Conference on Advanced Networks and Telecommunications Systems*, 2024.